

Northumbria Research Link

Citation: Mansouri, Seyed Amir, Nematbakhsh, Emad, Ahmarinejad, Amir, Jordehi, Ahmad Rezaee, Javadi, Mohammad Sadegh and Marzband, Mousa (2022) A hierarchical scheduling framework for resilience enhancement of decentralized renewable-based microgrids considering proactive actions and mobile units. *Renewable and Sustainable Energy Reviews*, 168. p. 112854. ISSN 1364-0321

Published by: Elsevier

URL: <https://doi.org/10.1016/j.rser.2022.112854>
<<https://doi.org/10.1016/j.rser.2022.112854>>

This version was downloaded from Northumbria Research Link:
<https://nrl.northumbria.ac.uk/id/eprint/49799/>

Northumbria University has developed Northumbria Research Link (NRL) to enable users to access the University's research output. Copyright © and moral rights for items on NRL are retained by the individual author(s) and/or other copyright owners. Single copies of full items can be reproduced, displayed or performed, and given to third parties in any format or medium for personal research or study, educational, or not-for-profit purposes without prior permission or charge, provided the authors, title and full bibliographic details are given, as well as a hyperlink and/or URL to the original metadata page. The content must not be changed in any way. Full items must not be sold commercially in any format or medium without formal permission of the copyright holder. The full policy is available online: <http://nrl.northumbria.ac.uk/policies.html>

This document may differ from the final, published version of the research and has been made available online in accordance with publisher policies. To read and/or cite from the published version of the research, please visit the publisher's website (a subscription may be required.)

A hierarchical scheduling framework for resilience enhancement of decentralized renewable-based microgrids considering proactive actions and mobile units

Seyed Amir Mansouri ^{1*}, Emad Nematbakhsh ², Amir Ahmarinejad ³,
Ahmad Rezaee Jordehi⁴, Mohammad Sadegh Javadi ⁵, Mousa Marzband^{6,7}

¹ Department of Electrical Engineering, Yadegar-e-Imam Khomeini (RAH) Shahre Rey Branch, Islamic Azad University, Tehran, Iran

² Faculty of Electrical Engineering, University of Isfahan, Isfahan, Iran

³ Department of Electrical Engineering, Central Tehran Branch, Islamic Azad University, Tehran, Iran

⁴ Department of Electrical Engineering, Rasht Branch, Islamic Azad University, Rasht, Iran

⁵ Institute for Systems and Computer Engineering, Technology and Science (INESC TEC), Porto, Portugal

⁶ Department: Mathematics, Physics and Electrical Engineering, Northumbria University, UK

⁷ Center of Research Excellence in Renewable Energy and Power Systems, King Abdulaziz University, Jeddah, 21589, Saudi Arabia

Abstract

Nowadays, decentralized microgrids (DC-MGs) have become a popular topic due to the effectiveness and the less complexity. In fact, DC-MGs resist to share their internal information with the distribution system operator (DSO) to protect their privacy and compete in the electricity market. Further, lack of information sharing among MGs in normal operation conditions leads to form a competitive market. However, in emergency operation conditions, it results numerous challenges in managing network outages. Therefore, this paper presents a hierarchical model consisting of three stages to enhance the resilience of DC-MGs. In all stages, the network outage management is performed considering the reported data of MGs. In the first stage, proactive actions are performed with the aim of increasing the network readiness against the upcoming windstorm. In the second stage, generation scheduling, allocation of mobile units and distribution feeder reconfiguration (DFR) are operated by DSO to minimize operating costs. In the final stage, the repair crew is allocated to minimize the energy not served (ENS). Uncertainties of load demand, wind speed and solar radiation are considered, and the effectiveness of the proposed model is investigated by integrating to the 118-bus distribution

* Corresponding Author: Amir.mansouri24@gmail.com

network. Finally, the results of the simulation indicate that DFR and proactive actions decrease the ENS by 19,124 kWh and 4,101 kWh, respectively. Further, the sharing of information among MGs leads to a 48.16% growth in the supply service level to critical loads, and consequently a 3.47% increase in the resilience index.

Highlights

- Presenting a hierarchical framework for distribution system resilience enhancement
- Increasing network readiness through performing proactive actions
- Sending mobile units to sensitive nodes to reduce ENS and accelerate system recovery
- Reducing ENS in critical consumers through data sharing among DC-MGs
- Reducing computational burden by dividing the problem to the three-stage

Keywords: Decentralized Microgrids; Renewable Energy Sources; Resilience Enhancement; Distribution Feeder Reconfiguration; Mobile Emergency Units.

Word Count: 11369

List of Abbreviations

CL	Critical load
DC-MGs	Decentralized Microgrids
DFR	Distribution feeder reconfiguration
DR	Demand response
DSO	Distribution system operator
ENS	Energy not served
ESS	Energy storage system
MEG	Mobile emergency generator
MESS	Mobile energy storage system
MG	Microgrid
MILP	Mixed-integer linear programming
OC	Operation cost
RC	Repair crew
RER	Renewable energy resource
RI	Resilience index
RL	Regular load
TSO	Transmission system operator
$B_{i,j}^{Line}$	Line susceptance (S)

$C_{e,t,s}^{ESS}$	ESS operation cost (\$)
$C_{g,t,s}^{Gen}$	Gas turbine operation cost (\$)
$C_{i,t}^{MEG} / C_{i,t}^{MESS}$	Mobile unit's operation cost (\$)
ct	Crew teams index
$d_{r,s'}$	Distance between scenario pairs
$D_{n,m,ct}^{CT}$	Transportation path status (crew team)
$D_{m,n,meg/mess}^{MEG/MESS}$	Transportation path status (MEG/MESS)
$D_{n,m,rc}^{RC}$	Transportation path status (repair crew)
$E_e^{initial}$	Initial energy of ESS (kWh)
E_e^{min} / E_e^{max}	Min/Max energy of ESS (kWh)
$E_{e,t,s}$	ESS energy (kWh)
e	ESS Index
EP	Proactive action time (min.)
$G_{pv,t,s}$	Irradiance (W/m ²)
G_{std}	Irradiance in STC (W/m ²)
$G_{i,j}^{Line}$	Line conductance (S)
g	Gas turbine index
$I_{e,t,s}^{ch} / I_{e,t,s}^{dch}$	Charge/Discharge status
i,j	Electrical bus
$k_{i,j,t,s}$	Power flow direction status
l	Line index
M	Large positive number
meg	MEG index
$mess$	MESS index
$N_n^{MEG/MESS,Max}$	Max MEG/MESS allocation
n,m	Transportation point index
$pd_{r,s'}$	Production of probability and distance values
$P_{meg}^{Max} / Q_{meg}^{Max}$	Active/Reactive capacity of mobile DGs (kW/kVar)
$P_{e,t,s}^{ch,Max} / P_{e,t,s}^{dch,Max}$	ESS charge/discharge limits (kW)
$P_{e,t,s}^{ch} / P_{e,t,s}^{dch}$	ESS charge/discharge power (kW)
$P_{i,t}^{Demand} / Q_{i,t}^{Demand}$	Electrical load (kW/kVar)
$P_{i,t,s}^{ENS} / Q_{i,t,s}^{ENS}$	ENS (kW/kVar)
P_g^{Min} / P_g^{Max}	Gas turbine active power generation limits (kW)
$P_{g,t,s}^{Gen} / Q_{g,t,s}^{Gen}$	Gas turbine power generation (kW/kVar)
$P_{t,s}^{Sub} / Q_{t,s}^{Sub}$	Main grid power generation (kW/kVar)
P_{pv}^r / P_w^r	Max solar/wind power (kW)
$P_{i,t}^{MEG} / P_{i,t}^{Dch,MESS} / Q_{i,t}^{MGen}$	Mobile unit's power generation (kW/kVar)
$P_{i,t,s}^{Demand,RL} / P_{i,t,s}^{Demand,CL}$	Regular/Critical load (kW)
$P_{i,t,s}^{ENS,RL} / P_{i,t,s}^{ENS,CL}$	ENS of regular/critical load (kW)
$P_{pv,t,s}^{PV} / P_{w,t,s}^{Wind}$	Solar panel's/Wind turbine's power generation (kW)
$\tilde{P}_{(...)}$	Upper-level results (kW)

$P_{i,j,t,s}^{Line} / Q_{i,j,t,s}^{Line}$	Power flow (kW/kVar)
$P_{i,j,t,s}^{Loss}$	Power loss (kW)
pv	Solar generation index
Q_g^{Min} / Q_g^{Max}	Gas turbine reactive power generation limits (kVar)
$r_{i,j}$	Line resistance (Ω)
rc	Repair crew index
$S_{i,j}^{Max}$	Line capacity (kVA)
$S_{i,j,t,s}^{Line}$	Power flow (kVA)
s	Scenario index
$T_{n,ct}^{CT}$	Crew team's travel time (min.)
T_i^M	Mobile unit's installation Time (min.)
\tilde{t}	Number of time order
$T_{n,rc}^{RC}$	Repair crew's travel time (min.)
T_m^R	Repairing time (min.)
t_1 / t_2	Start/End programming time
T_m^{SW}	Switching time (min.)
t	Time index
$T_{n,m}^{Travel} / T_{n,i}^{Travel}$	Travel time (min.)
$T_{i,meg/mess}^{MEG/MESS}$	Travel time of mobile units (min.)
$u_{i,t,mg}$	Mobile unit's operation status
v^{cri} / v^{col}	Critical/Collapse wind speed (m/s)
v_s	Wind speed (m/s)
$V_{i,t,s}^{Bus}$	Voltage magnitude (p.u.)
V^{Min} / V^{Max}	Voltage magnitude limits (p.u.)
w	Wind turbine index
$x_{i,j}$	Automatic/Manual switch installation
$x_{i,j}$	Line reactance (ohm)
$y_{i,j,t,s}$	Line's status
$\alpha_{n,m}^{Traffic}$	Traffic delay
δ^{Max}	Max switching number
Δ	Time step
$\delta_{i,j,t,s}$	Switching status
ε	Small positive number
$\eta_e^{ch} / \eta_e^{dch}$	Efficiency of ESS charge/discharge (%)
η^{PV}	PV panel efficiency (%)
γ_{mg}	Penalty cost (\$/kWh)
$\lambda_{l,s}$	Failure probability
λ_l^0	Standard failure probability
$\mu_{i,j,mg}$	Power exchange weight
$\omega^{RL} / \omega^{CL}$	Regular/Critical load weight
$\varphi_{mg}^{RL} / \varphi_{mg}^{CL}$	Regular/Critical load weight of MGs
π^{EES}	ESS operation cost (\$/kWh)

$\pi_i^{ENS,RL} / \pi_i^{ENS,CL}$	ENS penalty of regular/critical loads (\$/kWh)
π_g^{Gen}	Gas turbine cost (\$/kWh)
π^{MEG} / π^{MESS}	Mobile unit's cost (\$/kWh)
π_t^M	Up-stream grid price (\$/kWh)
ρ_s	Scenario probability (%)
$\sigma_{n,i,mg}$	Mobile unit's allocation status
$\theta_{i,t,s}^{Bus}$	Voltage angle (rad)
$\theta^{Min} / \theta^{Max}$	Voltage angle limits (rad)
ξ_i^{Bus}	Active-Reactive power ratio (%)

1. Introduction

1.1. Background and Motivation

In recent years, improving the resilience of electric power systems against extreme weather events has become one of the main concerns of researchers as these events occur more frequent. However, as most of the distribution systems are designed to operate under normal condition, these events could result serious damages to the distribution systems. [1]. Therefore, numerous short-term and long-term measures have been investigated in recent years to deal with these events. Long-term measures include hardening of the distribution system, placement of sectionalizing switches and backup generators, while short-term measures include proactive actions, distribution feeder reconfiguration, allocation of mobile emergency units (generators and storage systems), and execution of demand response (DR) programs [2]. This study focuses on short-term measures to deal with high impact low probability events.

Proactive actions include pre-positioning of mobile units and crew teams, and implementing DFR to deal with upcoming events [3]. Further, multiple studies have shown that the deployment of mobile units and crew teams at network stations in the pre-disturbance phase could reduce the load shedding and increase the network recovery in the post-disturbance phase. DFR is also one of the most effective approaches to enhance the resilience of distribution systems. Consequently, DFR reroutes power flow by changing the status of manual and automatic switches, thus leading to enhanced system resilience. Therefore, in this model,

proactive actions including pre-positioning of mobile units and DFR are performed to enhance the system resilience during emergency conditions.

Nowadays, one of the trending topics in the field of distribution systems is the resilience enhancement of the active distribution network in multiple MGs. These MGs consist of distributed energy resources (DERs) and energy storage systems (ESSs) that supply the load of their customers through their DERs and purchases from upstream grid. Further, MGs can operate in both on-grid and off-grid modes [4].

In modern distribution systems with several MGs, the system operator faces many challenges to improve network resilience than traditional distribution systems, because these MGs resist to share their internal information. This has motivated the authors of this paper to provide a hierarchical framework to enhance the resilience of a 118-bus distribution system consisting of 8 MGs, which investigates the effect of MG data sharing on system resilience.

1.2. Literature Review

In recent years, several studies have been conducted with the aim of enhancing the resilience of MGs to deal with extreme weather conditions. For instance, in Ref. [5], a multi-stage stochastic model is presented to improve the resilience of interconnected MGs, **in which AC power flow constraints are considered.** In this study, electric vehicles participate in load supply during emergency conditions, and the results demonstrate that the proposed model significantly reduces the solution time by dividing the operation problem into a multi-stage problem. In Ref. [6], optimal size of MESSs have been determined to enhance the resilience of DC-MGs. Further, the optimization problem is modeled as a three-level problem and solved by adaptive genetic algorithm (GA). Moreover, uncertainties due to load demand and DERs output power were considered in the model and the results indicate that the proposed model leads to improved system resilience by determining the exact size of MESSs. Authors in Ref. [7] use the potential of electric vehicles (EVs) to improve the resilience of MGs under emergencies. In this study,

each MG first reports information about the amount of energy stored in its EVs to the central control system, and then the central control system sends the EVs to islanded MGs. Further the simulation results indicate that the proposed method leads to enhanced system resilience.

Many studies in recent years have shown that connecting MEGs and MESSs to vital nodes during emergency conditions could reduce load shedding in the system. Besides, several studies have shown that performing proactive actions in the pre-disturbance phase has a great impact on the recovery speed of the network. In this regard, in Ref. [8], the effect of proactive actions on system resilience and recovery speed has been investigated and the results indicate that timely pre-positioning of crew teams and MEGs leads to increased recovery speed. In addition, Ref. [9] indicates that performing proactive actions has improved the resilience of a 47-bus distribution system, and the results demonstrate that the predictability of upcoming events has a high impact on reducing the amount of load shedding in the system. Furthermore, Ref. [10] presents a stochastic MILP model to improve the resilience of a distribution network, in which the DSO changes the network topology during emergency conditions through manual and automatic switches. Moreover, the results of this study demonstrated that pre-positioning of service teams and MEGs in the pre-disturbance phase could lead to a reduction in load shedding. In Ref. [11], the problem of resilience enhancement of a 33-bus distribution system in the presence of residential, industrial and agricultural loads is investigated. In particular, back up diesel generators, MESSs and DR programs have been used to enhance the system resilience and the results demonstrate that this model has led to a 16.5% reduction in operating costs during emergency condition. Further, Ref. [12] presents a model based on deep reinforcement learning for the planning of distribution system hardening over a 100-year horizon. The optimization problem is modeled as a Markov decision process and it is solved by integrating novel ranking strategy, neural networks, and reinforcement learning. Finally, the simulation results show that the proposed model has increased the system resilience by 30%.

Moreover, Ref. [13] proves that the installation of ESS on sensitive nodes of the network along with hardening of lines significantly improves system resilience. In Ref. [14], the discharge of not-in-service electric buses has been utilized to improve the resilience of a distribution system during emergencies. In fact, the objective function of this model is to minimize the load shedding and the results show that electric buses as temporary mobile power sources have a high potential to increase the speed of system recovery.

In addition, numerous studies have proven that DFR is one of the most effective approaches to enhance the system resilience during emergency conditions. Further, DFR is performed through changing the status of manual and automatic switches [15]. The optimal placement of sectionalizing switches is performed in Ref. [16] to enhance the resilience of a 33-bus distribution system. In particular, the uncertainties of fault occurrence, generation of renewable energy resources (RERs) and load demand are considered to accomplish the operation conditions in the model. In the proposed strategy, DSO changes the network topology and forms several self-sufficient MGs to prevent the spread of faults in the network. Finally, the results confirm that reconfigurable topology and the formation of MGs optimize the resilience under emergency conditions. In Ref. [16], a two-layer method based on the model predictive control is presented, in which the structure of each MG is determined in the first layer and the second layer performs DERs scheduling. Thereafter, the two-layer model is transformed into a one-layer optimization problem by strong duality theory and implemented on the 37-bus distribution system. The results define that the proposed method has improved the resilience of the distribution system during the outage of DERs. Moreover, Ref. [17] presents a MILP model for network outage management which apply DFR to enhance the resilience. The rank-based constraint is considered to guarantee the radiality of the network structure during DFR, and the model is implemented on the 69-bus and the 123-bus distribution networks. Finally, the results indicate that the proposed strategy reduces load shedding in emergency situations.

1.3. Research Gap and Contribution

The comprehensive review of the above literatures has illustrated that most studies have examined the problem of resilience enhancement in a centralized MGs and only a limited number of research have examined the resilience enhancement of DC-MGs. Further, Table 1 provides a detailed comparison between this study and recent papers. It expresses that the proposed model in this work is considered the impact of proactive actions, mobile units' deployment, reconfigurable topology, and data sharing on the resilience enhancement of DC-MGs, while other papers have considered only some of these items in their model. Overall, this paper presented a hierarchical model consisting of three stages for enhancing the resilience of decentralized networks, where the outage management of the main network is functioned by considering the MGs data. In the first stage, proactive actions are performed to increase the network readiness to deal with the upcoming windstorm. In the second stage, generation scheduling, allocation of mobile units and DFR are fulfilled by DSO and according to the MGs data. Ultimately, in the third stage, the damaged lines are repaired. In general, the main contributions of this paper could be highlighted as follow:

- Presenting a hierarchical framework for distribution system resilience enhancement in the presence of DC-MGs
- Increasing network readiness through performing proactive actions
- Sending MEGs and MESSs to sensitive nodes of the network to reduce ENS and speed up system recovery
- Reducing ENS of critical consumers through data sharing among DC-MGs
- Reducing computational burden by dividing the optimization problem into a three-stage model
- Employing a scenario-based method for modeling load demand, wind speed and solar radiation uncertainties

Table 1. Comparison between the proposed model and previous papers.

Refs.	MGs	Proactive Actions	Mobile Units		Crews		DFR	ESS	DR	RER	Uncertainty	Fault Scenarios	Load Priority	Data Sharing
			MEG	MESS	Switching	Repair								
[18]	x	x	✓	✓	x	✓	x	x	x	x	x	✓	✓	x
[19]	✓	x	✓	x	x	x	x	✓	x	✓	✓	x	x	x
[20]	x	x	x	✓	x	x	x	✓	x	✓	✓	x	✓	x
[11]	x	x	x	✓	x	x	x	✓	✓	✓	✓	x	✓	x
[21]	x	x	x	x	x	✓	x	x	x	x	x	✓	x	x
[22]	x	x	x	x	x	✓	✓	x	x	x	x	x	x	x
[23]	x	x	✓	x	x	x	✓	x	x	x	✓	✓	✓	x
[24]	✓	x	✓	x	x	✓	x	✓	x	x	✓	✓	✓	x
[25]	x	x	x	x	x	x	x	x	x	x	✓	✓	x	x
[26]	✓	x	x	x	x	x	x	✓	x	✓	✓	x	x	x
[27]	✓	✓	x	x	x	x	x	✓	x	x	x	x	x	x
[28]	✓	x	x	x	x	x	x	x	x	x	x	x	x	x
[6]	✓	✓	x	✓	x	x	x	✓	x	✓	✓	✓	x	x
[29]	✓	x	x	x	x	x	✓	✓	✓	✓	✓	x	✓	x
[30]	x	x	✓	x	x	✓	✓	x	x	x	x	✓	x	x
[31]	✓	✓	x	✓	x	✓	x	x	x	✓	✓	✓	✓	x
[32]	✓	x	x	x	x	x	✓	✓	x	x	x	x	x	x
[33]	x	✓	x	✓	x	✓	x	x	x	x	x	✓	x	x
[34]	x	x	x	x	x	x	✓	✓	✓	✓	✓	x	✓	x
This Paper	✓	✓	✓	✓	✓	✓	✓	✓	✓	✓	✓	✓	✓	✓

2. Model Development

2.1. System Description

Figure 1 depicts the modified 118-bus IEEE distribution system studied in this paper, and the information on network is in accordance with Ref. [35]. Furthermore, this network consists of 8 MGs that are operated in a decentralized manner and each MG supplies its consumers through DERs and network purchases. Consequently, an ESS is installed next to each RES. The network is equipped with five MEGs and four MESSs, which are connected to vital buses to participate in load supply in case of an emergency. Moreover, in the proposed model, DSO is able to change the network topology through manual (on-site control) and automatic (remote control) switches. In this regard, five crew teams are considered that are dispatched to the location of the manual switches to change the status. Moreover, as it can be seen in the Fig. 1, the network is divided into three regions and the wind speed is varying in each of them. In the proposed model, wind speed is considered constant along the entire region. Note that the solar radiation is assumed to be different in each region, so that the maximum values of radiation in regions 1 to 3 are 500 W/m^2 , 450 W/m^2 and 400 W/m^2 respectively [36].

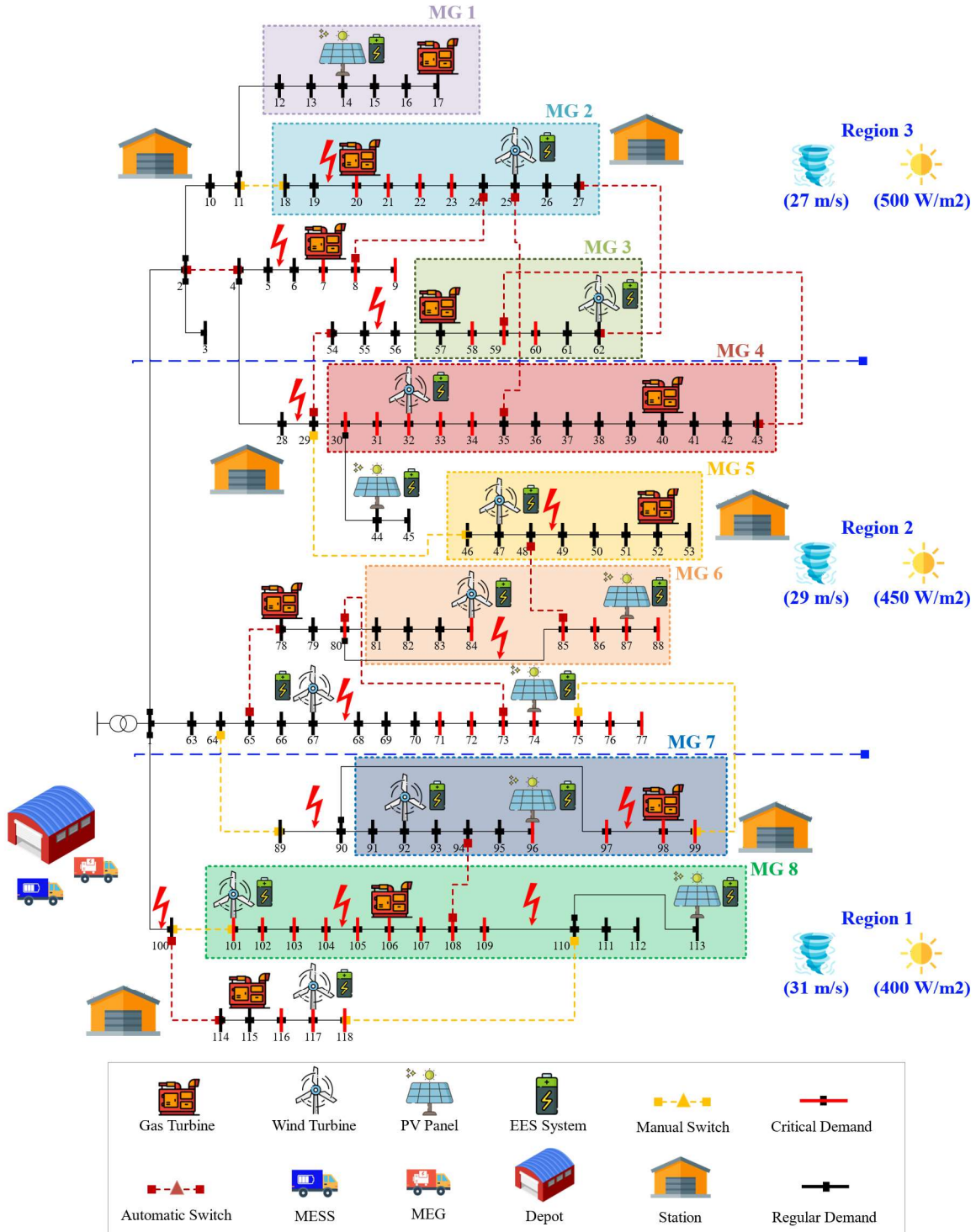


Fig. 1. Modified IEEE 118-bus distribution system structure.

2.2. Mathematical Modeling

In this section, the proposed hierarchical framework is formulated as a MILP optimization problem. In fact, the first stage represents the pre-disturbance phase while the second and third

stages represent the post-disturbance phase. Further, Figure 2 shows that at each stage of the proposed model, the scheduling problems of MGs and the main grid are modeled in the form of a bi-level optimization problem. It can also be seen, that the scheduling problem of MGs is solved in a decentralized manner, and in all three stages, the scenario-based method has been utilized to model the uncertainties of load demand, wind speed and solar radiation.

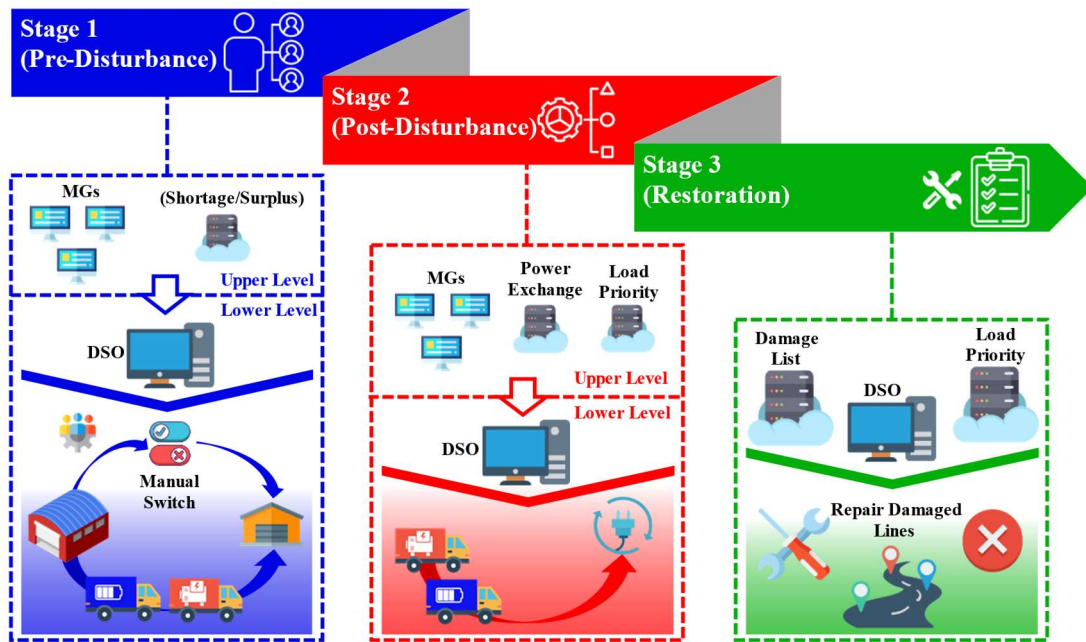


Fig. 2. The structure of the proposed model.

- **Stage 1**

In the first stage of the proposed study, proactive actions are performed for maximizing load supply to deal with upcoming windstorm threats. At this stage, the operation problem is solved for fault scenarios. In particular, the fault scenarios are generated through the fragility function and the predicted speed for the upcoming windstorm.

Equations (1) and (2) respectively represent the objective functions of MGs and DSO in the first stage. According to Eq. (1), at the upper-level, each MG schedules to maximize the load supply and reports its power shortage/surplus to the DSO. Then at the lower-level (according to Eq. 2), the DSO plans the entire network according to the data reported by the MGs to optimize the load supply. Moreover, at this stage DSO changes the network topology through

manual and automatic switches based on fault scenarios and also sends mobile units from the depot to the stations.

$$\max Load_{mg}^{Supply} = \sum_{s=1}^S \rho_s \left[\begin{aligned} & \varphi_{mg}^{RL} \sum_{i=1}^{I_{mg}} \sum_{t=1}^T (P_{i,t,s}^{Demand,RL} - P_{i,t}^{ENS,RL}) \\ & + \varphi_{mg}^{CL} \sum_{i=1}^{I_{mg}} \sum_{t=1}^T (P_{i,t,s}^{Demand,CL} - P_{i,t}^{ENS,CL}) \end{aligned} \right] \quad (1)$$

$$\max Load_{DSO}^{Supply} = \sum_{s=1}^S \rho_s \left[\begin{aligned} & \varphi_{DSO}^{RL} \sum_{i=1}^{I_{DSO}} \sum_{t=1}^T (P_{i,t,s}^{Demand,RL} - P_{i,t}^{ENS,RL}) \\ & + \varphi_{DSO}^{CL} \sum_{i=1}^{I_{DSO}} \sum_{t=1}^T (P_{i,t,s}^{Demand,CL} - P_{i,t}^{ENS,CL}) \\ & + \sum_{t=1}^T \sum_{(i,j)=1}^{L_{mg}} \mu_{i,j,mg} |P_{i,j,t,s}^{Line} - \tilde{P}_{i,j,t,s}^{Line}| \end{aligned} \right] \quad (2)$$

- **Stage 2**

The second stage of this work is solved as a bi-level optimization problem in the post-disturbance phase. In fact, at this stage, the problem is solved for the most probable scenario of fault and by considering the uncertainties of load demand, wind speed and solar radiation. In the upper-level, the MGs plan their next hours with to minimize the operating costs and report their power exchange data to the DSO. Then, at the lower-level, the DSO plans the entire network with regard to data by MGs for reducing the operating cost. Moreover, the DSO at this level performs network scheduling by allocating mobile units and implementing DFR.

Equation (3) states that the objective function of each MG is to minimize the cost of purchasing power from the grid, the operating cost of DERs, the operating cost of ESS, and the ENS penalty. In addition, Eq. (4) defines that the DSO objective function is to minimize the cost of purchasing power from the upstream network, the operating cost of network equipment, the operating cost of mobile units, the penalty for ENS and the penalty for not observing schedules of MGs.

$$\min C_{mg} = \sum_{t=1}^T \left[\pi_t^M \left(\sum_{(i,j)=1}^{L_{mg}} \mu_{i,j,mg} P_{i,j,t}^{Line} \right) \right] + \sum_{g=1}^{G_{mg}} \sum_{t=1}^T C_{g,t}^{Gen} + \sum_{e=1}^{E_{mg}} \sum_{t=1}^T C_{e,t}^{ESS} + \sum_{i=1}^{I_{mg}} \sum_{t=1}^T C_{i,t}^{ENS} \quad (3)$$

$$\begin{aligned}
\min C^{DSO} = & \sum_{t=1}^T (\pi_t^M P_t^{Sub}) + \sum_{g=1}^{G_{DSO}} \sum_{t=1}^T C_{g,t}^{Gen} + \sum_{e=1}^{E_{DSO}} \sum_{t=1}^T C_{e,t}^{ESS} \\
& + \sum_{i=1}^I \sum_{t=1}^T (C_{i,t}^{MEG} + C_{i,t}^{MESS}) + \sum_{i=1}^{I_{DSO}} \sum_{t=1}^T C_{i,t}^{ENS} \\
& + \sum_{mg=1}^{MG} \gamma_{mg} \left[\sum_{t=1}^T \sum_{(i,j)=1}^{L_{mg}} \mu_{i,j,mg} |P_{i,j,t}^{Line} - \tilde{P}_{i,j,t}^{Line}| \right. \\
& \left. + \sum_{i=1}^{I_{mg}} \sum_{t=1}^T (\varphi_{mg}^{RL} |P_{i,t}^{ENS,RL} - \tilde{P}_{i,t}^{ENS,RL}| + \varphi_{mg}^{CL} |P_{i,t}^{ENS,CL} - \tilde{P}_{i,t}^{ENS,CL}|) \right]
\end{aligned} \tag{4}$$

- **Stage 3**

At this stage, DSO sends repair crews to the damaged lines locations. Particularly, the repair crews are equipped between 14:00 and 15:30 and then at 15:30 DSO sends them to the location of damaged lines. Moreover, Eq. (5) shows that the DSO objective function at this level is to minimize the penalty for ENS and the penalty for not observing schedules of MGs.

$$\begin{aligned}
\min C^{DSO} = & \sum_{i=1}^{I_{DSO}} \sum_{t=1}^T C_{i,t}^{ENS} \\
& + \sum_{mg=1}^{MG} \gamma_{mg} \left[\sum_{t=1}^T \sum_{(i,j)=1}^{L_{mg}} \mu_{i,j,mg} |P_{i,j,t}^{Line} - \tilde{P}_{i,j,t}^{Line}| \right. \\
& \left. + \sum_{i=1}^{I_{mg}} \sum_{t=1}^T (\varphi_{mg}^{RL} |P_{i,t}^{ENS,RL} - \tilde{P}_{i,t}^{ENS,RL}| + \varphi_{mg}^{CL} |P_{i,t}^{ENS,CL} - \tilde{P}_{i,t}^{ENS,CL}|) \right]
\end{aligned} \tag{5}$$

- **Power Flow Constraints**

All stages of the proposed model are solved by considering linear AC power flow constraints to prevent overflows in branches of the network. These constraints can be found in Eqs. (a1)-(a9) [37]. The susceptance and conductance of each line are calculated through Eqs. (a1) and (a2), respectively. Further, active and reactive power flow in each line are calculated via Eqs. (a3) and (a4), respectively, which are a function of the susceptance, conductance, voltage magnitude and its angle [37]. The apparent power of each line is also calculated via Eq. (a5), which depends on the active and reactive power flow in that line, while Eq. (a6) limits the apparent power of each line. The binary variable $y_{i,j,t,s}$ determines the active/inactive state of

each line at scenario s and time t , which is multiplied by a large positive number (M) to prevent the constraint (a6) from being applied to inactive lines. Eqs. (a7) and (a8) are used to calculate the magnitude and angle of the voltage at bus i and time t , respectively. Lastly, the losses of each line are calculated via Eq. (a9) [38].

$$B_{i,j}^{Line} = \frac{x_{i,j}}{r_{i,j}^2 + x_{i,j}^2} \quad (a1)$$

$$G_{i,j}^{Line} = \frac{r_{i,j}}{r_{i,j}^2 + x_{i,j}^2} \quad (a2)$$

$$P_{i,j,t,s}^{Line} = G_{i,j}^{Line} (V_{i,t,s}^{Bus} - V_{j,t,s}^{Bus}) + B_{i,j}^{Line} (\theta_{i,t,s}^{Bus} - \theta_{j,t,s}^{Bus}) + \frac{P_{i,j,t,s}^{Loss}}{2} \quad (a3)$$

$$Q_{i,j,t,s}^{Line} = B_{i,j}^{Line} (V_{j,t,s}^{Bus} - V_{i,t,s}^{Bus}) + G_{i,j}^{Line} (\theta_{i,t,s}^{Bus} - \theta_{j,t,s}^{Bus}) \quad (a4)$$

$$S_{i,j,t,s}^{Line\ 2} = P_{i,j,t,s}^{Line\ 2} + Q_{i,j,t,s}^{Line\ 2} \quad (a5)$$

$$-S_{i,j}^{Max} - M(1 - y_{i,j,t,s}) \leq S_{i,j,t,s}^{Line} \leq S_{i,j}^{Max} + M(1 - y_{i,j,t,s}) \quad (a6)$$

$$V^{Min} \leq V_{i,t,s} \leq V^{Max} \quad (a7)$$

$$\theta^{Min} \leq \theta_{i,t,s} \leq \theta^{Max} \quad (a8)$$

$$P_{i,j,t,s}^{Loss} = r_{i,j} \left[\left(P_{i,j,t,s}^{Line} \right)^2 + \left(Q_{i,j,t,s}^{Line} \right)^2 \right] \quad (a9)$$

- **Switching Constraints**

Constraints (b1)-(b4) allow the DSO to perform DFR [39]. In this regard, changing the status of lines equipped with switches is specified through inequalities (b1) and (b2). In fact, these constraints state that if the status of the switch changes at time t , the value of its binary variable ($\delta_{i,j,t,s}$) becomes 1. The number of switching is restricted via Eq. (b3). Finally, the constraint (b4) indicates that the network topology could be changed only through the lines equipped with the switch.

$$-\delta_{i,j,t,s} \leq y_{i,j,t,s} - y_{i,j,t-1,s} \leq \delta_{i,j,t,s} \quad (b1)$$

$$\delta_{i,j,t,s} \leq y_{i,j,t,s} + y_{i,j,t-1,s} \leq 2 - \delta_{i,j,t,s} \quad (b2)$$

$$0 \leq \sum_{t=1}^T \delta_{i,j,t,s} \leq \delta^{Max} \quad (b3)$$

$$\sum_{t=1}^T \delta_{i,j,t,s} \leq x_{i,j} M \quad (b4)$$

- **Radiality Constraints**

Constraints (c1)-(c3) guarantee the radial structure of the network topology during DFR [40]. In particular, the constraint (c1) identifies parent buses, and it states that if the value of $k_{i,j,t,s}$ is 1, the power flow direction is from bus i to bus j , and vice versa. Furthermore, each bus could be connected to a parent bus at most, which is modeled by constraint (c2). Finally, constraint (c3) is imposed to prevent the slack bus from connecting to the parent buses.

$$0 \leq k_{i,j,t,s} + k_{j,i,t,s} \leq y_{i,j,t,s} \quad (c1)$$

$$\sum_{j=1}^J k_{j,i,t,s} \leq 1 \quad (c2)$$

$$\sum_{j=1}^J k_{j,i=1,t,s} = 0 \quad (c3)$$

- **Load Control Constraints**

Load control constraints are given in (d1)-(d7). In fact, constraints (d1) and (d2) state that the amount of ENS of normal and critical consumers at bus i and time t must be equal to or less than the load demand of these consumers at same bus and time. Equation (d3) expresses that the load of each bus could contain both normal and critical loads, while Eq. (d4) states that the ENS of each bus could contain the ENS of normal and critical consumers. The constraint (d5) balances the interruption of active and reactive loads. ζ_i^{Bus} is the ratio of active to reactive load at each node. Moreover, the ENS penalty is calculated by Eq. (d6), which is a function of the type of load and its penalty. Finally, the resilience index of the system is calculated using Eq. (d7). This index is the ratio of the amount of load supplied between t_1 to t_2 to the total amount of demand within this period. In addition, RI index will be equal to 1 when MG can fully supply its load. ω^{RL} and ω^{CL} are weighted coefficients that determine the value of normal and critical loads, respectively.

$$0 \leq P_{i,t,s}^{ENS,RL} \leq P_{i,t}^{Demand,RL} \quad (d1)$$

$$0 \leq P_{i,t,s}^{ENS,CL} \leq P_{i,t}^{Demand,CL} \quad (d2)$$

$$P_{i,t,s}^{Demand} = P_{i,t,s}^{Demand,RL} + P_{i,t,s}^{Demand,CL} \quad (d3)$$

$$P_{i,t,s}^{ENS} = P_{i,t,s}^{ENS,RL} + P_{i,t,s}^{ENS,CL} \quad (d4)$$

$$P_{i,t,s}^{ENS} = \xi_i^{Bus} Q_{i,t,s}^{ENS} \quad (d5)$$

$$C_{i,t,s}^{ENS} = \left(\pi_i^{ENS,RL} P_{i,t,s}^{ENS,RL} + \pi_i^{ENS,CL} P_{i,t,s}^{ENS,CL} \right) \Delta t \quad (d6)$$

$$RI = \frac{\sum_{t=t_1}^{t_2} \omega^{CL} \left(P_{i,t,s}^{Demand,CL} - P_{i,t,s}^{ENS,CL} \right) + \omega^{RL} \left(P_{i,t,s}^{Demand,RL} - P_{i,t,s}^{ENS,RL} \right)}{\sum_{t=t_1}^{t_2} P_{i,t,s}^{Demand}} \quad (d7)$$

• DERs Operating Constraints

Equation (e1) indicates that the power generated by PV panel is a function of solar radiation at scenario s and time t , standard radiation, panel capacity and efficiency [41]. Further, Eq. (e2) indicates that the power generated by wind turbine is calculated through a three-part function. The first part states that, if the wind speed in scenario s and time t is outside the acceptable range of the turbine, the output power will be zero. The second part of the function states that, if the wind speed at time t is within the range $v_i \leq v_{w,t,s} < v_r$, the power generated by the turbine is calculated through given function. The third part of this function expresses that, if the wind speed at time t is within the range $v_r \leq v_{w,t,s} < v_o$, the power generated by the turbine is equal to its rated power. v_i , $v_{w,t,s}$, v_r and v_o are cut-in speed, wind speed at time t , rated speed and cut-out speed, respectively. Active and reactive power generated by gas turbine are limited by constraints (e3) and (e4), respectively, while the operation cost of the gas turbine is calculated via Eq. (e5).

$$P_{pv,t,s}^{PV} = \frac{G_{pv,t,s}}{G_{std}} P_{pv}^r \eta^{PV} \quad (e1)$$

$$P_{w,t,s}^{Wind} = \begin{cases} 0, & v_{w,t,s} < v_i, v_{w,t,s} \geq v_o \\ P_w^r \frac{v_{w,t,s} - v_i}{v_r - v_i}, & v_i \leq v_{w,t,s} < v_r \\ P_w^r, & v_r \leq v_{w,t,s} < v_o \end{cases} \quad (e2)$$

$$P_g^{Min} \leq P_{g,t,s}^{Gen} \leq P_g^{Max} \quad (e3)$$

$$Q_g^{Min} \leq Q_{g,t,s}^{Gen} \leq Q_g^{Max} \quad (e4)$$

$$C_{g,t,s}^{Gen} = \pi_g^{Gen} P_{g,t,s}^{Gen} \Delta t \quad (e5)$$

- **ESS Constraints**

ESS constraints (f1)-(f7) are incorporated into model. Particularly, constraint (f1) limits the level of energy stored in the ESS, whereas the hourly charge and discharge values of the ESS are limited by constraints (f2) and (f3), respectively. Further, constraint (f4) prevents simultaneous charging and discharging of the ESS. The energy level of the ESS at the current hour is calculated by Eq. (f5) [42], while constraint(f6) states that the energy level of the initial hour must be equal to a predetermined value. In addition, constraint (f7) indicates that the energy level of the ESS in the final hour must be equal to or greater than its energy level in the initial hour. Lastly, the operating cost of ESS is calculated via Eq. (f8).

$$E_e^{\min} \leq E_{e,t,s} \leq E_e^{\max} \quad (f1)$$

$$P_{e,t,s}^{Ch} \leq P_{e,t,s}^{Ch,Max} I_{e,t,s}^{Ch} \quad (f2)$$

$$P_{e,t,s}^{Dch} \leq P_{e,t,s}^{Dch,Max} I_{e,t,s}^{Dch} \quad (f3)$$

$$0 \leq I_{e,t,s}^{Ch} + I_{e,t,s}^{Dch} \leq 1 \quad (f4)$$

$$E_{e,t,s,y} = E_{e,t-1,s} + \left(P_{e,t,s}^{Ch} \eta_e^{Ch} - \frac{P_{e,t,s,y}^{Dch}}{\eta_e^{Dch}} \right) \Delta t \quad (f5)$$

$$E_{e,t=0,s} = E_e^{predetermined} \quad (f6)$$

$$E_{e,t=0,s} \leq E_{e,t=24,s} \quad (f7)$$

$$C_{e,t,s}^{ESS} = \pi^{ESS} \left(P_{e,t,s}^{Ch} + P_{e,t,s}^{Dch} \right) \Delta t \quad (f8)$$

- **Crew Team Deployment in Pre-Disturbance Phase**

Equation (g1)–(g11) present the constraints required for modeling routing of crew teams in the pre-disturbance phase. The time required to travel and change the status of each manual switch is calculated using Eq. (g1). In fact, $T_{n,ct}^{CT}$ and $T_{n,m}^{Travel}$ denote the time of presence at point n and the travel time between points n and m , respectively; T_m^{SW} represents the time required to change the status of the switch; the binary variable $D_{n,m,ct}^{CT}$ determines the travel path of crew teams. For example, if the crew team is dispatched from origin n to destination m , $D_{n,m,ct}^{CT}$

becomes 1. It is worth noting that the delay due to traffic ($\alpha_{n,m}^{Traffic}$) is also considered in the model. The constraint (g2) expresses that changing the status of manual switches is only possible if crew teams are dispatched to those locations, while constraint(g3) ensures that crew teams leave the depot in the pre-disturbance phase. Further, constraint (g4) deploys crew teams at stations, whereas constraint (g5) prevents crew teams from returning to the depot. Besides, to ensure the presence of crew teams in the station at the end of the pre-disturbance phase, constraint (g6) is provided. Constraint (g7) expresses that crew team must leave the site after switching, while constraint(g8) states that only one team can be dispatched to the switch location. Moreover, Eq. (g9) calculates the switching time. According to Eq. (g10), if the crew team does not travel to point n , the value of its binary variable ($T_{n,ct}^{CT}$) becomes 0. Ultimately, Eq. (g11) expresses that the crew could only leave point n if they have been sent to that point.

A simplified model is used to model the transportation system between origin and destination points of crew teams and mobile units, [39]. Figure 3 presents the three steps of modelling phrases. In the first step, the length of the lines is calculated based on their resistance. In the second step, the coordinates of origin and destination points are determined and the distance between the origin and destination points are calculated as a straight line, in the third step.

$$T_{n,ct}^{CT} + T_{n,m}^{Travel} \alpha_{n,m}^{Traffic} + T_m^{SW} - (1 - D_{n,m,ct}^{Crew}) M \leq T_{m,ct}^{CT} \quad (g1)$$

$$\leq T_{n,ct}^{CT} + T_{n,m}^{Travel} \alpha_{n,m}^{Traffic} + T_m^{SW} + (1 - D_{n,m,ct}^{CT}) M \quad (g2)$$

$$\sum_{m=1}^M \sum_{ct=1}^{CT} D_{m,n,ct}^{CT} = \sum_{(i,j)=n}^L \sum_{t=1}^T \delta_{i,j,t} \quad (g3)$$

$$\sum_{m=1}^M D_{n,m,ct}^{CT} = 1 \quad (g4)$$

$$\sum_{m=1}^M D_{m,n,ct}^{CT} = 1 \quad (g5)$$

$$\sum_{m=1}^M D_{m,n,ct}^{CT} = 0 \quad (g6)$$

$$T_{n,ct}^{CT} \leq EP \quad (g7)$$

$$\sum_{m=1}^M D_{n,m,ct}^{CT} = \sum_{m=1}^M D_{m,n,ct}^{CT} \quad (g7)$$

$$0 \leq \sum_{m=1}^M \sum_{ct=1}^{CT} D_{m,n,ct}^{CT} \leq 1 \quad (g8)$$

$$\sum_{ct=1}^{CT} T_{n,c}^{CT} \leq \sum_{(i,j)=n}^L \sum_{t=1}^T \delta_{i,j,t} \tilde{t} \leq \sum_{ct=1}^{CT} T_{n,c}^{CT} + \Delta t - \varepsilon \quad (g9)$$

$$T_{n,ct}^{CT} \leq \sum_{m=1}^M D_{m,n,ct}^{CT} M \quad (g10)$$

$$\sum_{m=1}^M D_{n,m,ct}^{CT} \leq \sum_{m=1}^M D_{m,n,ct}^{CT} \quad (g11)$$

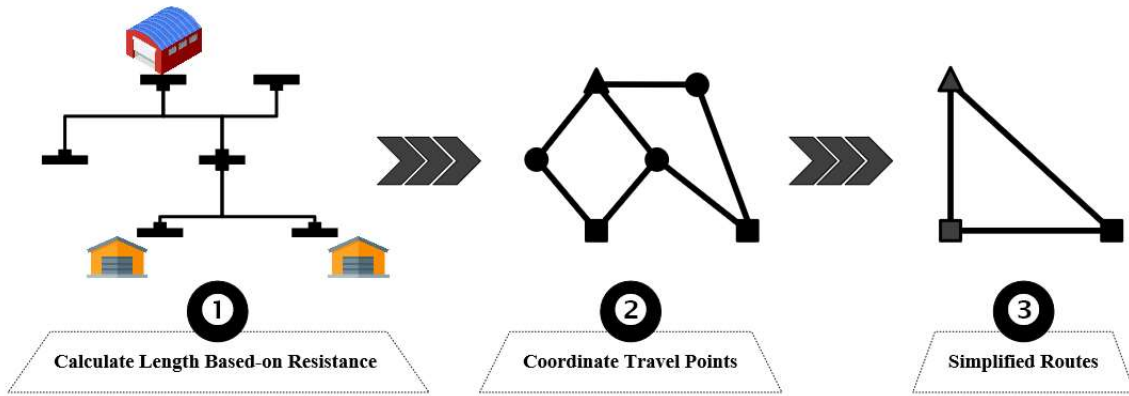


Fig. 3. Simplified transportation system.

- **Crew Team Constraints in Post-Disturbance Phase**

The routing constraints of the crew teams in the post-disturbance phase (stages two and three) are the same as the constraints introduced for the pre-disturbance phase (stage one) and only the travel direction is different. Further, in the post-disturbance phase, crew teams are dispatched from the stations to the location of manual switches and return to the depot after changing the status of the switches. In this regard, constraints (g3)-(g5) with (h1)-(h3) and constraints (g10)-(g11) with (h4)-(h5) are replaced.

$$\sum_{m=1}^M D_{n,m,ct}^{CT} = 1 \quad (h1)$$

$$\sum_{m=1}^M D_{m,n,ct}^{CT} = 1 \quad (h2)$$

$$\sum_{m=1}^M D_{m,n,ct}^{CT} = 0 \quad (h3)$$

$$T_{n,ct}^{CT} \leq \sum_{m=1}^M D_{m,n,ct}^{CT} M \quad (h4)$$

$$\sum_{m=1}^M D_{n,m,ct}^{Crew} \leq \sum_{m=1}^M D_{m,n,ct}^{Crew} \quad (h5)$$

- **Repair Crew**

Equations (11)-(19) are provided to model repair crew routing at stage three [43]. In fact, these constraints are similar to the routing constraints of crew teams and only the indices and variables are different. Moreover, the repair crews are equipped between 14:00 and 15:30 and then dispatched to the location of damaged lines with the aim of ENS penalty minimization. Eventually, after repairing all the damaged lines, the repair crews return to the depot.

$$T_{n,rc}^{RC} + T_{n,m}^{Travel} \alpha_{n,m}^{Traffic} + T_m^R - (1 - D_{n,m,rc}^{RC}) M \leq T_{m,rc}^{RC} \quad (i1)$$

$$\leq T_{n,rc}^{RC} + T_{n,m}^{Travel} \alpha_{n,m}^{Traffic} + T_m^R + (1 - D_{n,m,rc}^{RC}) M$$

$$\sum_{m=1}^M \sum_{rc=1}^{RC} D_{m,n,rc}^{RC} = \sum_{(i,j)=n}^L \sum_{t=1}^T \delta_{i,j,t} \quad (i2)$$

$$\sum_{m=1}^M D_{n,m,rc}^{RC} = 1 \quad (i3)$$

$$\sum_{m=1}^M D_{m,n,rc}^{RC} = 1 \quad (i4)$$

$$\sum_{m=1}^M D_{n,m,rc}^{RC} = \sum_{m=1}^M D_{m,n,rc}^{RC} \quad (i5)$$

$$0 \leq \sum_{m=1}^M \sum_{rc=1}^{RC} D_{m,n,rc}^{RC} \leq 1 \quad (i6)$$

$$\sum_{rc=1}^{RC} T_{n,rc}^{RC} \leq \sum_{(i,j)=n}^L \sum_{t=1}^T \delta_{i,j,t} \tilde{t} \leq \sum_{rc=1}^{RC} T_{n,rc}^{RC} + \Delta t - \varepsilon \quad (i7)$$

$$T_{n,rc}^{RC} \leq \sum_{m=1}^M D_{m,n,rc}^{RC} M \quad (i8)$$

$$\sum_{m=1}^M D_{n,m,rc}^{RC} \leq \sum_{m=1}^M D_{m,n,rc}^{RC} \quad (i9)$$

- **Mobile Units Allocation Constraints**

The equations for pre-positioning of mobile units in the pre-disturbance phase are presented in (j1)-(j4) [9]. In the pre-disturbance phase, mobile units are sent from the depot to the stations. Equation (j1) presents the limitation of sending mobile units to each station, while constraint (j2) is provided to prevent the deployment of each mobile unit in more than one station. In addition, time of mobile units is calculated using Eq. (j3), while constraint (j4) guarantees the deployment of mobile units at stations before the event.

$$\sum_{meg/mess=1}^{MEG/MESS} D_{m=depot,n,meg/mess}^{MEG/MESS} \leq N_n^{MEG/MESS,Max} \quad (j1)$$

$$\sum_{n=1}^{N_{Stations}} D_{m=depot,n,meg/ess}^{MEG/MESS} = 1 \quad (j2)$$

$$T_{n,m,meg/mess}^{MEG/MESS} = T_{n,m}^{Travel} D_{n,m,meg/mess}^{MEG/MESS} \quad (j3)$$

$$T_{n,m,meg/mess}^{MEG/MESS} \leq EP \quad (j4)$$

- **Mobile Units Operating Constraints**

Constraints required for the allocation and operation of mobile units in the post-disturbance phase are given in Eqs. (k1)-(k11) [44]. In this phase, mobile units are sent from stations to the buses. In fact, Eq. (k1) states that the dispatch of mobile units from station n to bus i is subject to their presence at the station. Further, constraint (k2) indicates that only one mobile unit could be sent to each bus, while constraint(k3) states that the injection of power by mobile units in each bus is subject to the presence of these units in the related buses. Constraint (k4) states that the mobile unit can only inject power into the grid after dispatch and connection to the bus, whereas Eq. (k5) calculates the time required to travel from station n to bus i and connect to it. In addition, the limitations on the amount of active and reactive power generated by MEG are presented in constraints (k6)-(k7), respectively. Constraint (k8) restricts the hourly discharge of MESS, while constraint(k9) states that the total energy discharged from the MESS must be less than or equal to the energy stored in it. Finally, the operating costs of MEGs and MESSs are calculated via Eqs. (k10) and (k11), respectively.

$$\sum_{i=1}^I \sigma_{n,i,meg/mess} \leq D_{m=depot,n,meg/mess}^{MEG/MESS} \quad (k1)$$

$$0 \leq \sum_{n=1}^{N_{Stations}} \sum_{meg/mess=1}^{MEG/MESS} \sigma_{n,i,meg/mess} \leq 1 \quad (k2)$$

$$0 \leq u_{i,t,meg/mess} \leq \sum_{n=1}^{N_{stations}} \sigma_{n,i,meg/mess} \quad (k3)$$

$$u_{i,t,meg/mess} \tilde{t} \geq T_{i,meg/mess}^{MEG/MESS} - (1 - u_{i,t,meg})M \quad (k4)$$

$$\begin{aligned} T_{n,meg/mess}^{MEG/MESS} + T_{n,i}^{Travel} \alpha_{n,i}^{Traffic} + T_i^M - (1 - \sigma_{n,i,meg/mess})M &\leq T_{i,meg/mess}^{MEG/MESS} \\ &\leq T_{n,meg/mess}^{MEG/MESS} + T_{n,i}^{Travel} \alpha_{n,i}^{Traffic} + T_i^M + (1 - \sigma_{n,i,meg/mess})M \end{aligned} \quad (k5)$$

$$0 \leq P_{i,t}^{MEG} \leq \sum_{meg=1}^{MEG} P_{meg}^{Max} u_{i,t,meg} \quad (k6)$$

$$0 \leq Q_{i,t}^{MEG} \leq \sum_{meg=1}^{MEG} Q_{meg}^{Max} u_{i,t,meg} \quad (k7)$$

$$0 \leq P_{i,t}^{Dch,MESS} \leq \sum_{mess=1}^{MESS} P_{mess}^{Dch,Max} u_{i,t,mess} \quad (k8)$$

$$0 \leq \sum_{t=1}^T P_{i,t}^{Dch,MESS} \Delta t \leq \sum_{n=1}^{N_{Stations}} \sum_{mess=1}^{MESS} \sigma_{n,i,mess} E_{mess}^{Initial} \quad (k9)$$

$$C_{i,t}^{MEG} = \pi^{MEG} P_{i,t}^{MEG} \Delta t \quad (k10)$$

$$C_{i,t}^{MESS} = \pi^{MESS} P_{i,t}^{MESS} \Delta t \quad (k11)$$

- **Power Balance Constraints in Pre-Disturbance Phase**

Active and reactive power balance constraints in the pre-disturbance phase are presented in Eqs. (11) and (12), respectively. These constraints guarantee the balance of power generation and consumption per bus.

$$\begin{aligned} P_{t,s}^{Sub} \Big|_{i=1} &+ \sum_{g=1}^{G_i} P_{g,t,s}^{Gen} + \sum_{pv=1}^{PV_i} P_{pv,t,s}^{PV} + \sum_{w=1}^{W_i} P_{w,t,s}^{Wind} + \sum_{e=1}^{E_t} (P_{e,t,s}^{Dch} - P_{e,t,s}^{Dh}) \\ &= \sum_{l(i,j)=1}^L P_{i,j,t,s}^{Line} + P_{i,t}^{Demand} - P_{i,t,s}^{ENS} \end{aligned} \quad (11)$$

$$Q_{t,s}^{Sub} \Big|_{i=1} + \sum_{g=1}^{G_i} Q_{g,t,s}^{Gen} = \sum_{(i,j)=1}^L Q_{i,j,t,s}^{Line} + Q_{i,t,s}^{Demand} - Q_{i,t,s}^{ENS} \quad (12)$$

- **Power Balance Constraints in Post-Disturbance Phase**

In Eqs. (m1) and (m2), the active and reactive power balance constraints in the post-disturbance phase are presented. Further, the mobile units participate in supplying the load, the active and reactive power balance constraints are rewritten considering the power injected by these units.

$$\begin{aligned}
P_t^{Sub} \Big|_{i=1} &+ \sum_{g=1}^{G_i} P_{g,t}^{Gen} + P_{i,t}^{MEG} + P_{i,t}^{Dch,MESS} + \sum_{pv=1}^{PV_i} P_{pv,t}^{solar} + \sum_{w=1}^{W_i} P_{w,t}^{wind} + \sum_{e=1}^{E_i} (P_{e,t}^{dch} - P_{e,t}^{ch}) \\
&= \sum_{l(i,j)=1}^L P_{i,j,t}^{Line} + P_{i,t}^{Demand} - P_{i,t}^{ENS}
\end{aligned} \tag{m1}$$

$$Q_t^{Sub} \Big|_{i=1} + \sum_{g=1}^{G_i} Q_{g,t}^{Gen} + Q_{i,t}^{MEG} = \sum_{(i,j)=1}^L Q_{i,j,t}^{Line} + Q_{i,t}^{Demand} - Q_{i,t}^{ENS} \tag{m2}$$

- **Scenario Generation and Reduction**

As mentioned above, the first stage of the proposed model is solved by considering fault scenarios arising from upcoming events. In this regard, 1000 fault scenarios are generated by the fragility function and according to the speed and path predicted for the storm. Thereafter, the number of initial scenarios is reduced to 10 by the backward scenario reduction algorithm to reduce the computational burden, In Eq. (n1), the failure probability of each line is calculated according to the wind speed in that area [45]. Where, $\lambda_{l(i,j)}^0$ is the failure probability of a standard line; μ , σ and Φ are the mean, standard division and log-normal distribution function, respectively; The values of μ , σ are equal to 0 and 0.25, respectively. v^{cri} And v^{col} denote critical and collapse velocities, accordingly.

In Eq. (n2), the status of each line (damaged/normal) is determined respect to the failure probability obtained. further, this function states that if the failure probability of line l is greater than a random value (r), that line is broken, and vice versa. In addition, this random value is generated for scenario s and time t by the uniform distribution function. Finally, the function given in Eq. (n3) states that the status of line l at the current hour depends on its status at the previous hour.

$$\lambda_{l(i,j),t} = \begin{cases} \lambda_{l(i,j)}^0, & v_{l(i,j),t} \leq v^{cri} \\ \Phi\left(\frac{v_{l(i,j),t} - \mu}{\sigma}\right), & v^{cri} < v_{l(i,j),t} \leq v^{col} \\ 1, & v_{l(i,j),t} > v^{col} \end{cases} \quad (n1)$$

$$\varphi_{l(i,j),t,s} = \begin{cases} 0, & \lambda_{l(i,j),t} \leq r \\ 1, & \lambda_{l(i,j),t} > r \end{cases} \quad (n2)$$

$$a_{l(i,j),t,s} = \begin{cases} 1 \times a_{l(i,j),t-1,s}, & \varphi_{l(i,j),t,s} = 0 \\ 0 \times a_{l(i,j),t-1,s}, & \varphi_{l(i,j),t,s} = 1 \end{cases} \quad (n3)$$

3. Methodology

The solution method of the proposed hierarchical framework is illustrated in figure 4. Specifically, the developed MILP model is solved by the CPLEX solver in GAMS. According to the flowchart in the first step, scenario generation and reduction process is performed. Table 2 presents the pseudocode of this process. It is worth to mention that 1000 fault scenarios are generated by the fragility function. Further, 1000 scenarios for load demand, wind speed and solar radiation are generated through normal, Weibull and beta distribution functions, respectively. Moreover, to increase the solution speed, the scenarios generated for each parameter are reduced to 10 by the backward scenario reduction method [46].

In the second step, the first stage of the proposed model is solved. At this stage, proactive actions are performed in the pre-disturbance phase to maximize the load supply. Furthermore, the proactive actions include dispatching mobile units to stations and DFR. In the third step, the third stage of the proposed model is solved in the restoration phase. At this stage, the MGs firstly plan their upcoming hours with the aim of minimizing operating cost and report their power exchange data to the DSO. Thereafter, the DSO performs the final network scheduling, including generation planning, mobile units' allocation, and DFR, with observance of data reported by MGs, to optimize the operating cost. Ultimately, in the fourth step, the third stage

of the proposed model, which is the allocation of repair crews with the aim of minimizing the ENS penalty, is solved., where the solution process ends after repairing all damaged lines.

Table 2. Pseudocode to illustrate the generation and reduction process of fault scenarios.

Scenario Generation	Step 1	For each line l, do: For each time t, do: Calculate failure probability of each line l with fragility curve, Eq. (n1). End End
	Step 2	For each line l, do: For each time t, do: For each scenario s, do: Generate a random number r between 0 and 1 with uniform function for each time-based scenario. Define the damage status of each line l based-on failure probability, Eq. (n2). Calculate probability of each scenario based-on number of normal and damaged lines. End End End
	Step 3	For each line l, do: For each time t, do: For each scenario s, do Define availability status of each line l based-on the damage status from windstorm start time to t, Eq. (n3). End End End
Scenario Reduction	Step 4	For each scenario pair (s and s'), do: Compute the distance between s and s'. End
	Step 5	Find the scenario r with minimum distance from scenario s. Compute the <i>pd</i> value between scenario r and other scenarios. $pd_{r,s'} = \rho_s d_{r,s'}$ Find scenario d with minimum <i>pd</i> value.
	Step 6	Update the probability of scenario r. Remove scenario d from the set of scenarios. Update the set of scenarios.
	Step 7	If the required number of scenarios is achieved, Then: Return the set of scenarios. Else: Go To Step 4.

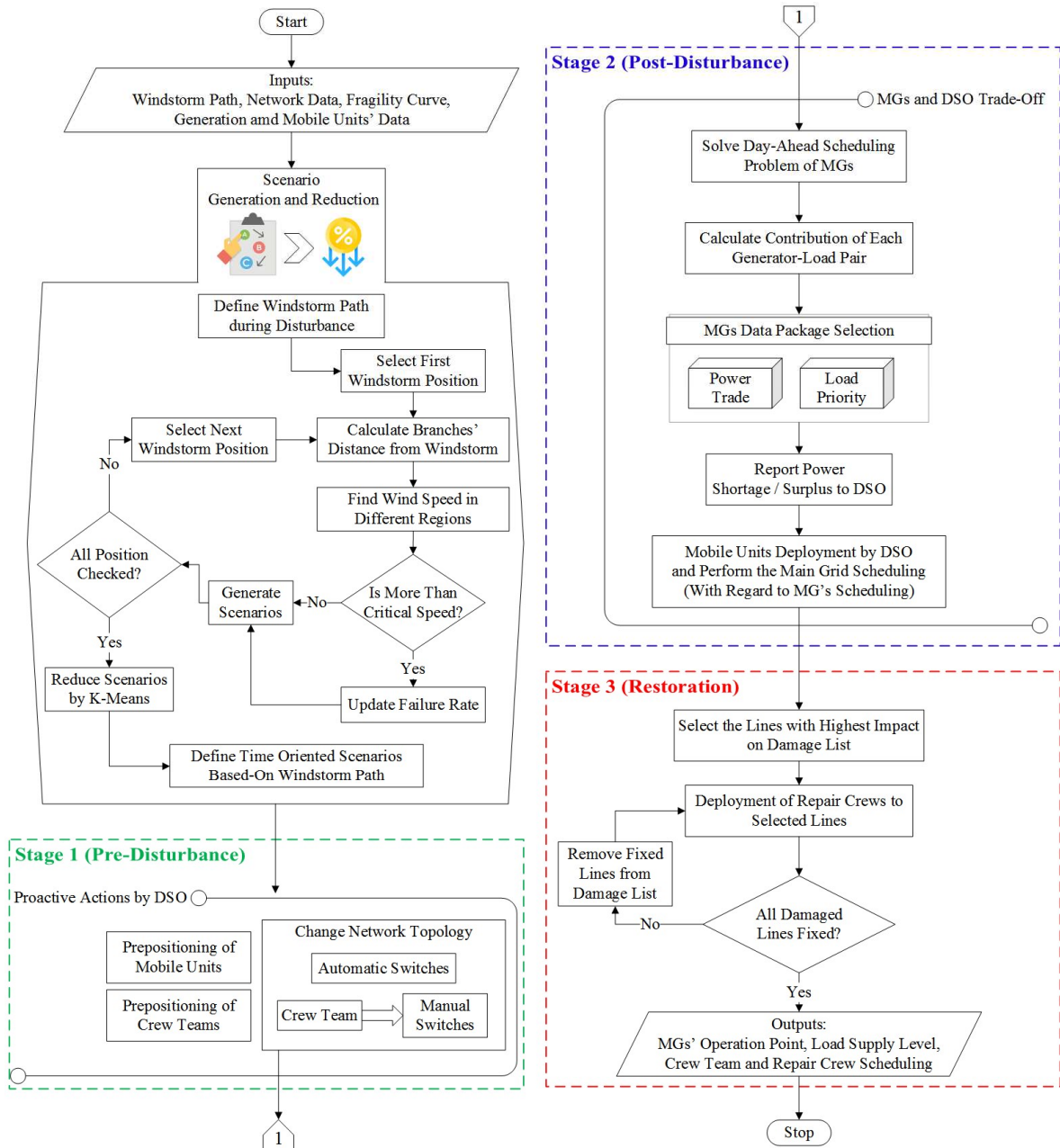


Fig. 4. Flowchart of the proposed hierarchical model.

4. Results

4.1. Input Data

In this section, the effectiveness of the proposed model is tested by implementing it on a modified IEEE 118-bus distribution system and solving 6 case studies. In fact, the problem is solved for a typical day in October, and the case studies are presented in Table 3. Moreover, the case studies have been selected to investigate the impacts of mobile units, proactive actions, reconfigurable topology, and data sharing among MGs on improving system resilience.

Furthermore, the power trade refers to the power exchange of each MG, while the load priority refers to the type of loads (regular or critical). Table 4 presents the data required to simulate the proposed model, whereas the obtained scenarios for faults are presented in Table 5. This table lists the line number on which the fault occurred, and the numbers in parentheses indicate the buses at both ends of the line. The scenarios of load, wind speed and solar radiation are depicted in Figs. 5a-5c, respectively. Finally, the price of electricity is according to Ref. [37].

Table 3. Case studies and their assumptions.

Case	Data Sharing by MGs		Reconfigurable Topology	MEGs	MESSs	Proactive Actions
	Power Trade	Load Priority				
1	✓	✗	✗	✗	✗	✗
2	✓	✗	✓	✗	✗	✗
3	✓	✗	✓	✓	✗	✗
4	✓	✗	✓	✓	✓	✗
5	✓	✗	✓	✓	✓	✓
6	✓	✓	✓	✓	✓	✓

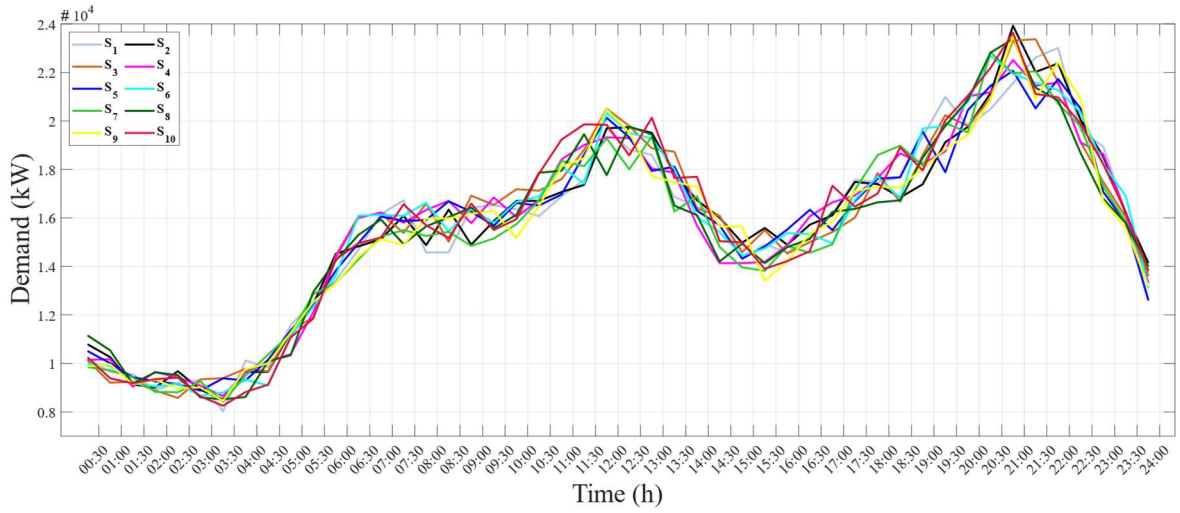
Table 4. Data required for simulating the proposed model.

Operation Parameters						
Stage 1 (h)	Stage 2 (h)	Stage 3 (h)	π_i^M (\$/kWh)	δ^{Max}	ε	M
10:00-14:00	14:00-15:30	15:30-23:00	0.25	40	1e-5	1e5
v_i (m/s)	v_r (m/s)	v_o (m/s)	γ_{mg} (\$/kW)	$\varphi_{mg}^{CL} / \omega^{CL}$	$\varphi_{mg}^{CL} / \omega^{CL}$	$\mu_{i,j,mg}$
2	14	26	5	2	1	1
G_{std} (W/m ²)	Q_g^{Min} / Q_g^{Max}	v^{cri} / v^{col} (m/s)	$\theta^{Min} / \theta^{Max}$	V^{Min} / V^{Max}	Δt (h)	η^{PV} (%)
1000	-60% / 60% P_g^{Max}	20/45	$-\pi / \pi$	0.9/1.1	1	95
γ_{mg} (\$/kWh)	λ_i^0 (%)	$\pi_i^{ENS,RL}$ (\$/kWh)	$\pi_i^{ENS,CL}$ (\$/kWh)	π^{MEG} (\$/kWh)	π^{MESS} (\$/kWh)	π_g^{Gen} (\$/kWh)
5	2	1	3	0.07	0.02	0.61
ESS Parameters						
η_e^{ch} (%)	η_e^{dch} (%)	$E_e^{initial}$ (%)	π^{ESS} (\$/kWh)	$P_{e,t,s}^{ch,Max}$ (%)	$P_{e,t,s}^{dch,Max}$ (%)	E_e^{min} / E_e^{max} (%)
95	95	50	0.02	40	40	20/90
Crew Teams & Repair Crew Parameters						
T_n^{SW} (min.)	T_n^R (min)	T_i^M (min.)	$\alpha_{n,m}^{Traffic}$	$N_n^{MEG/MESS,Max}$	EP (min)	
5	30	10	1.3	2	60	
Generation Units Parameters						

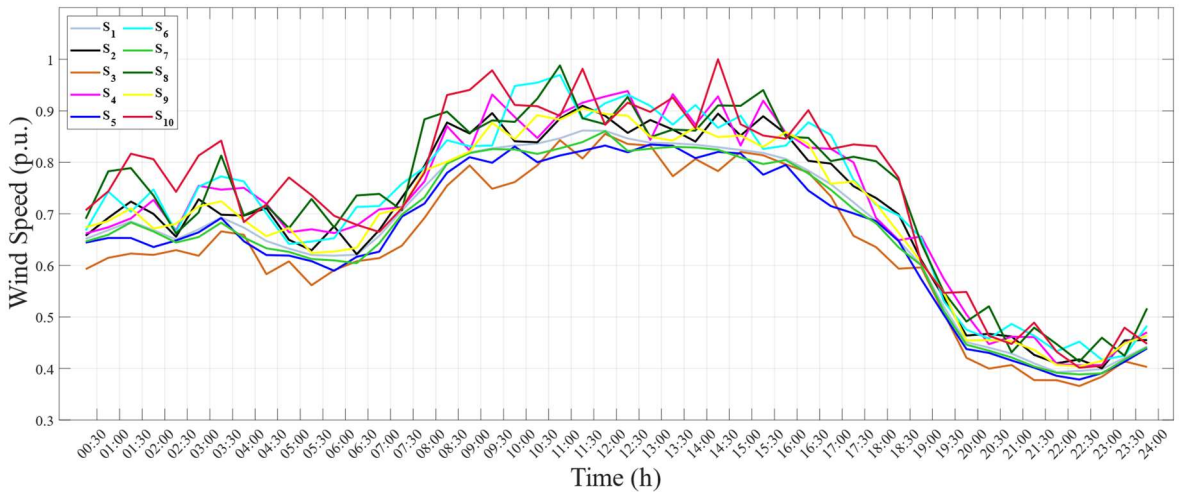
Wind Turbines Locations	Solar Panels Locations	Gas Turbines Locations
25 – 62 – 32 – 47 – 84 67 – 92 – 101 – 117	14 – 44 – 87 – 74 96 – 113	17 – 20 – 7 – 57 – 40 – 52 78 – 98 – 106 – 115
Capacity (kW)		
500 – 450 – 600 500 – 450 – 550 500 – 400 – 500	150 – 100 – 150 – 100 100 – 150	700 – 750 – 650 700 – 600 – 650 700 – 600 – 800 – 750

Table 5. Scenarios obtained for faults.

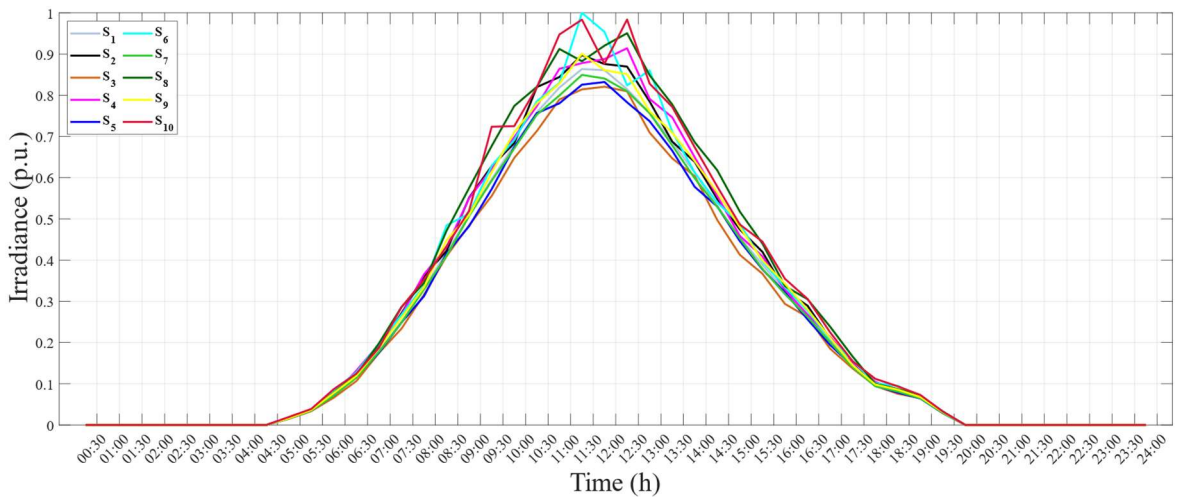
Scenario No.	1	2	3	4	5	6	7	8	9	10	
Line	32 (100-114)	98 (81-82)	46 (20-21)	49 (25-26)	94 (90-97)	45 (19-20)	113 (111-112)	89 (64-89)	36 (6-7)	65 (61-62)	
	68 (38-39)	112 (110-111)	33 (2-3)	82 (68-69)	5 (10-11)	35 (5-6)	27 (80-81)	11 (4-28)	52 (29-30)	86 (73-74)	
	55 (33-34)	111 (93)	100 (83-84)	97 (79-80)	55 (33-34)	60 (55-56)	67 (1)	67 (37-38)	46 (20-21)	124 (94-108)	
	20 (70-71)	(95-96)	65 (61-62)	73 (47-48)	5 (10-11)	51 (28-29)	1 (1-2)	112 (110-111)	99 (82-83)	108 (16-40-41)	
	76 (51-52)	(29-30)	71 (42-43)	80 (66-67)	123 (99-75)	74 (48-49)	113 (113)	34 (2-4)	18 (49-50)	95 (98-99)	
	119 (8-24)	(52-53)	87 (75-76)	36 (6-7)	66 (36-37)	28 (80-85)	30 (105-106)	30 (105-106)	114 (114-115)	105 (102-103)	
	14 (58-59)	(67-68)	12 (30-31)	106 (103-104)	115 (115-116)	81 (67-68)	106 (31)	106 (106)	37 (7-8)	103 (99-82-83)	
	114 (114-115)	(29-46)	110 (108-109)	104 (32-33)	116 (25-26)	22 (89-90)	109 (110)	106 (103-104)	63 (59-60)	99 (97-98)	
	70 (41-42)	(59-60)	109 (119)	80 (66-67)	112 (110-111)	97 (97-98)	81 (67-68)	104 (63)	99 (82-83)	25 (33-34)	
	54 (32-33)	(12-13)	13 (8-24)	106 (66-67)	111 (110-111)	107 (104-105)	39 (2-10)	39 (59-60)	20 (86)	86 (82-83)	
	20 (70-71)	(47-48)	(29-54)	103 (103-104)	33 (2-3)	105 (31)	105 (102-103)	105 (70-71)	30 (88)	2 (1-63)	
	32 (100-114)	(8-24)	(104-105)	35 (5-6)	115 (115-116)	115 (110-111)	112 (110-111)	112 (106)	17 (76-77)	41 (13-14)	
		(32-33)	115 (115-116)	51 (28-29)	116 (111-112)	3 (1-100)	3 (110-111)	83 (69-70)	17 (120)	17 (29-46)	
		5 (10-11)	116 (116)	70 (41-42)	112 (111-112)	113 (111-112)	120 (59-43)	120 (71)	112 (59-43)	57 (30-44)	
			2 (1-63)	56 (34-35)	51 (28-29)	51 (28-29)			112 (110-111)	73 (47-48)	
			66 (36-37)		79 (64-65)	79 (64-65)					
			82 (68-69)								
	Probability	0.076	0.091	0.16	0.153	0.094	0.164	0.017	0.144	0.059	0.042



(a) Load demand



(b) Wind speed



(c) Solar radiation

Fig. 5. Scenarios obtained for uncertain parameters.

4.2. Results of Cases 1 & 2

Tables 6 and 7 present the results of case studies 1 and 2, respectively. In fact, the network topology in cases 1 and 2 is assumed to be fixed and dynamic, respectively. Further, the results illustrate that in case 2 the total operation cost and ENS of the system are respectively reduced by 19.33% and 21.6% compared to case 1, due to the rerouting of power flow via DFR. In addition, Table 8 shows the open switches at each time step, and its analysis indicates that the network topology is changed 21 times. Moreover, Figure 6 depicts the load supply curve in cases 1 and 2. According to the figure, from 12:30 to 20:30 more load level is provided in case 2. It should be noted, that the reason for providing more load in case 2 is the possibility of extracting more power from DERs. Figures 7a and 7b depict the power injected into the network by RERs and gas turbines, respectively. Further, RERs and gas turbines have injected more power into the network in case 2. Therefore, the results prove that DFR leads to more use of DERs capacity and more load supply.

Table 6. Results obtained for the case 1.

Time Period		Pre-Disturbance (10:00-12:00)	During Disturbance (12:00-14:00)	Post-Disturbance (14:00-15:30)	Restoration (15:30-23:00)	Sum
MG 1	OC (\$)	-478.21	-443.43	-289.07	-691.72	-1902.43
	ENS (kWh)	0	0	0	0	0
MG 2	OC (\$)	81.72	3.37	176.35	814.44	1075.88
	ENS (kWh)	0	0	0	0	0
MG 3	OC (\$)	-544.71	105.72	0.17	20.59	-418.23
	ENS (kWh)	0	106.07	0	0	106.07
MG 4	OC (\$)	2310.44	10943.19	25617.59	115289.91	154161.1
	ENS (kWh)	0	1856.77	4715.42	21106.48	27678.67
MG 5	OC (\$)	188.25	1884.75	4139.08	18017.3	24229.38
	ENS (kWh)	0	396.03	859.87	3607.02	4862.92
MG 6	OC (\$)	296.07	3186.02	5701.86	21555.14	30739.09
	ENS (kWh)	0	447.71	816.94	3000.01	4264.66
MG 7	OC (\$)	98.77	8416.48	9350.57	22951.96	40817.78
	ENS (kWh)	0	1265.08	1397.41	3447.09	6109.58
MG 8	OC (\$)	2706.75	27643.72	22490.59	55876.3	108717.4
	ENS (kWh)	0	4969.58	4011.96	9173.69	18155.23
DSO	OC (\$)	6694.64	34329.1	36351.87	117457.62	194833.2
	ENS (kWh)	0	5015.96	5461.85	16880.89	27358.7
Sum	OC (\$)	11353.72	86068.92	103539.01	351291.54	552253.2
	ENS (kWh)	0	14057.2	17263.45	57215.18	88535.83

Table 7. Results obtained for the case 2.

Time Period		Pre-Disturbance (10:00-12:00)	During Disturbance (12:00-14:00)	Post-Disturbance (14:00-15:30)	Restoration (15:30-23:00)	Sum
MG 1	OC (\$)	-478.21	-437.73	-291.66	-697.93	-1905.53
	ENS (kWh)	0	0	0	0	0
MG 2	OC (\$)	81.72	1713.36	1211.04	5119.18	8125.3
	ENS (kWh)	0	304.14	246.65	924.45	1475.24
MG 3	OC (\$)	-544.71	-549.15	-399.61	-651.52	-2144.99
	ENS (kWh)	0	0	0	0	0
MG 4	OC (\$)	2310.44	2112.17	6121.51	75730.09	86274.21
	ENS (kWh)	0	67.5	708.36	11050.69	11826.55
MG 5	OC (\$)	188.25	4379.89	4265.55	17830.02	26663.71
	ENS (kWh)	0	919.51	888.31	3569.85	5377.67
MG 6	OC (\$)	296.07	5976.32	12158.62	20579.89	39010.9
	ENS (kWh)	0	1026.41	2164.98	3401.32	6592.71
MG 7	OC (\$)	98.77	5696.54	7312.96	40389.89	53498.16
	ENS (kWh)	0	904.76	1174.52	6280.5	8359.78
MG 8	OC (\$)	2706.75	26605.48	24758.64	52419.68	106490.6
	ENS (kWh)	0	3781.76	3599.09	7193.09	14573.94
DSO	OC (\$)	6694.64	13777.68	17693.44	91340.15	129505.9
	ENS (kWh)	0	2415.68	3377.82	15411.97	21205.47
Sum	OC (\$)	11353.72	59274.56	72830.49	302059.45	445518.2
	ENS (kWh)	0	9419.76	12159.73	47831.87	69411.36

Table 8. Status of switches in case 2.

Time Period	Open Switches								
	118 (27-62)	119 (8-24)	120 (59-43)	121 (48-85)	122 (80-73)	123 (99-75)	124 (94-108)	125 (118-110)	126 (25-35)
12:00	8 (11-18)	17 (29-46)	29 (100-101)	32 (100-114)	119 (8-24)	120 (59-43)	122 (80-73)	123 (99-75)	126 (25-35)
12:30	8 (11-18)	13 (29-54)	17 (29-46)	26 (65-78)	29 (100-101)	89 (64-89)	120 (59-43)	124 (94-108)	126 (25-35)
13:00	8 (11-18)	13 (29-54)	26 (65-78)	32 (100-114)	89 (64-89)	119 (8-24)	120 (59-43)	121 (48-85)	124 (94-108)
13:30	8 (11-18)	13 (29-54)	26 (65-78)	29 (100-101)	32 (100-114)	89 (64-89)	119 (8-24)	120 (59-43)	121 (48-85)
14:00	8 (11-18)	13 (29-54)	26 (65-78)	29 (100-101)	32 (100-114)	89 (64-89)	118 (27-62)	119 (8-24)	121 (48-85)
14:30	13 (29-54)	26 (65-78)	32 (100-114)	89 (64-89)	118 (27-62)	119 (8-24)	121 (48-85)	124 (94-108)	126 (25-35)
15:00	8 (11-18)	13 (29-54)	26 (65-78)	29 (100-101)	32 (100-114)	89 (64-89)	118 (27-62)	119 (8-24)	121 (48-85)
15:30	8 (11-18)	13 (29-54)	26 (65-78)	32 (100-114)	89 (64-89)	119 (8-24)	121 (48-85)	124 (94-108)	126 (25-35)
16:00	8 (11-18)	13 (29-54)	17 (29-46)	29 (100-101)	32 (100-114)	89 (64-89)	118 (27-62)	122 (80-73)	126 (25-35)
16:30	13 (29-54)	32 (100-114)	89 (64-89)	118 (27-62)	119 (8-24)	121 (48-85)	122 (80-73)	124 (94-108)	126 (25-35)
17:00	8 (11-18)	13 (29-54)	17 (29-46)	26 (65-78)	29 (100-101)	89 (64-89)	118 (27-62)	124 (94-108)	126 (25-35)
17:30	13 (29-54)	17 (29-46)	26 (65-78)	29 (100-101)	89 (64-89)	118 (27-62)	119 (8-24)	124 (94-108)	126 (25-35)
18:00	13 (29-54)	17 (29-46)	26 (65-78)	29 (100-101)	89 (64-89)	118 (27-62)	119 (8-24)	124 (94-108)	126 (25-35)

18:30	8 (11-18)	13 (29-54)	17 (29-46)	89 (64-89)	119 (8-24)	120 (59-43)	122 (80-73)	124 (94-108)	125 (118-110)
19:00	8 (11-18)	13 (29-54)	17 (29-46)	29 (100-101)	89 (64-89)	119 (8-24)	122 (80-73)	124 (94-108)	126 (25-35)
19:30	8 (11-18)	13 (29-54)	17 (29-46)	26 (65-78)	29 (100-101)	89 (64-89)	118 (27-62)	119 (8-24)	124 (94-108)
20:00	26 (65-78)	29 (100-101)	34 (2-4)	89 (64-89)	118 (27-62)	119 (8-24)	120 (59-43)	124 (94-108)	126 (25-35)
20:30	8 (11-18)	13 (29-54)	17 (29-46)	26 (65-78)	29 (100-101)	89 (64-89)	119 (8-24)	124 (94-108)	126 (25-35)
21:00	26 (65-78)	29 (100-101)	32 (100-114)	34 (2-4)	89 (64-89)	118 (27-62)	119 (8-24)	120 (59-43)	126 (25-35)
21:30	17 (29-46)	118 (27-62)	119 (8-24)	120 (59-43)	122 (80-73)	123 (99-75)	124 (94-108)	125 (118-110)	126 (25-35)
22:00	13 (29-54)	26 (65-78)	32 (100-114)	34 (2-4)	89 (64-89)	119 (8-24)	120 (59-43)	121 (48-85)	124 (94-108)
22:30	13 (29-54)	17 (29-46)	32 (100-114)	119 (8-24)	120 (59-43)	122 (80-73)	123 (99-75)	124 (94-108)	126 (25-35)
23:00	26 (65-78)	32 (100-114)	34 (2-4)	89 (64-89)	118 (27-62)	120 (59-43)	121 (48-85)	124 (94-108)	126 (25-35)

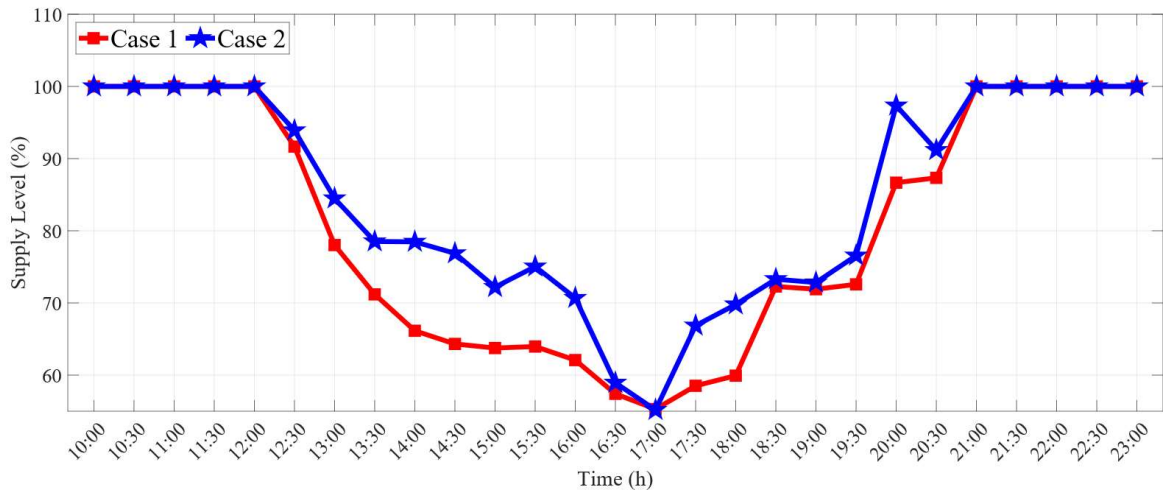
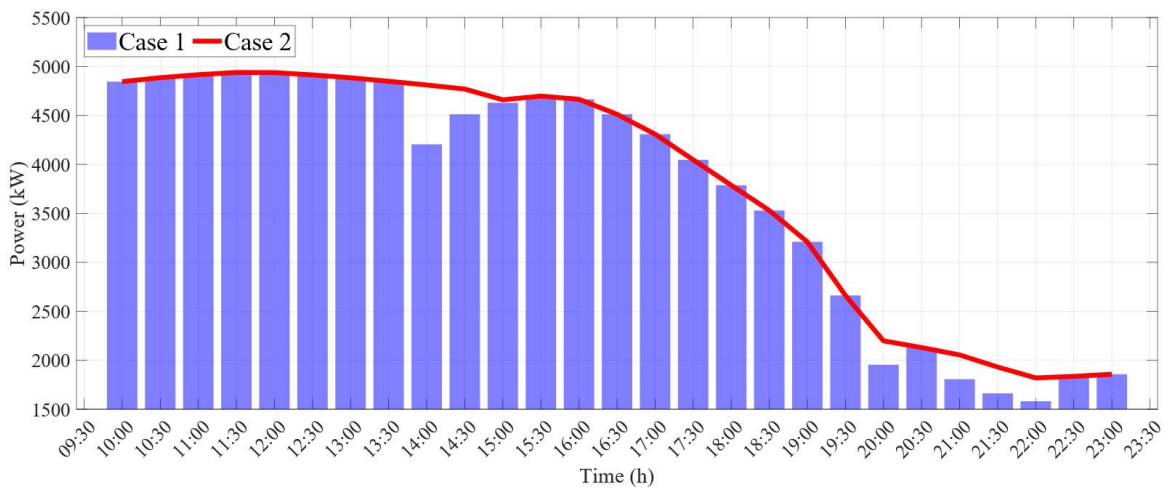
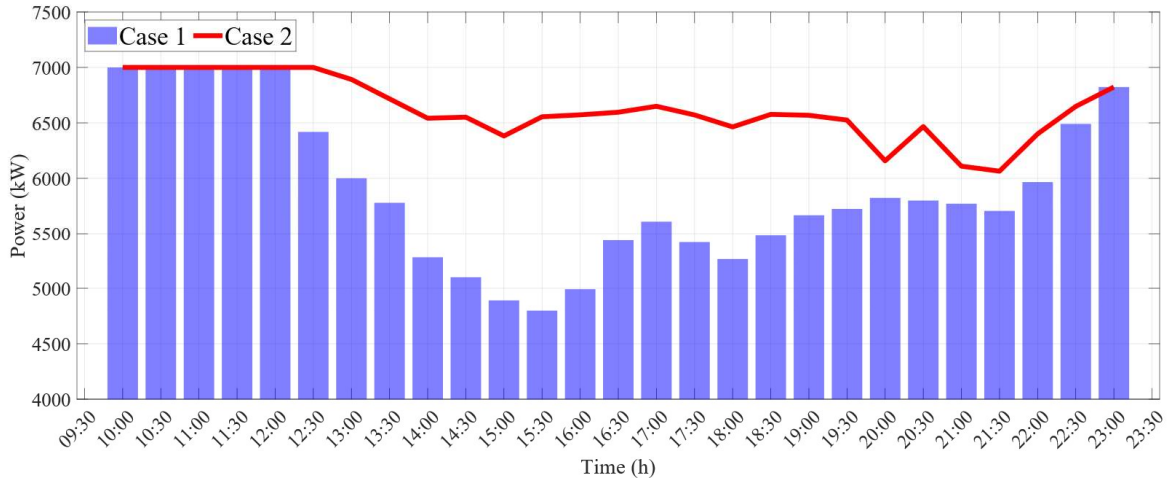


Fig. 6. Load supply curve in cases 1 and 2.



(a) RERs



(b) Gas turbines

Fig. 7. Power injected into the network by DERs in cases 1 and 2.

4.3. Results of Cases 3 & 4

Table 9 presents the results of case 3, and in the post-disturbance phase, MEGs are dispatched from the depot to the optimal buses and participate in the load supply. In fact, the results of this case indicate that the allocation of MEGs has led to a reduction in ENS and operation cost. Furthermore, numerical results illustrate that ENS and total operating cost are reduced by 27.16% and 23.5% compared to case 2, respectively. As shown in Fig. 8, after the occurrence of the disturbance (14:00), MEGs were dispatched from the depot to buses 45, 54, 75, 76, and 77 and participated in the load supply.

Table 10 presents the results obtained from case 4, and in addition to MEGs, MESSs are also dispatched from the depot to the optimal buses and participate in load supply. Moreover, the results of Table 10 illustrate that ENS and total operating cost decrease by 3.89% and 3.67% compared to case 3, respectively. Figure 9 depicts the scheduling obtained for MEGs and MESSs in case 4. Consequently, MEGs were sent to the buses 45, 55, 73, 74 and 90, while MESSs were to the buses 68, 71, 100 and 115.

Figure 10 compares the load supply curves in cases 2, 3 and 4. As can be observed, the level of load supply before and during disturbance in these cases is similar, while after connecting

the mobile units to the network the load supply level has dramatically increased in cases 3 and 4.

Table 9. Results obtained for the case 3.

Time Period		Pre-Disturbance (10:00-12:00)	During Disturbance (12:00-14:00)	Post-Disturbance (14:00-15:30)	Restoration (15:30-23:00)	Sum
MG 1	OC (\$)	-478.21	-437.73	-289.07	-715.62	-1920.63
	ENS (kWh)	0	0	0	0	0
MG 2	OC (\$)	81.72	1713.36	1220.88	5145.02	8160.98
	ENS (kWh)	0	304.14	246.65	924.45	1475.24
MG 3	OC (\$)	-544.71	-549.15	-389.26	-694.17	-2177.29
	ENS (kWh)	0	0	0	0	0
MG 4	OC (\$)	2310.44	2112.17	4810.64	56127.9	65361.15
	ENS (kWh)	0	67.5	513.82	7579.09	8160.41
MG 5	OC (\$)	188.25	4379.89	4508.5	18509.83	27586.47
	ENS (kWh)	0	919.51	939.33	3709.12	5567.96
MG 6	OC (\$)	296.07	5976.32	9511.29	10950.73	26734.41
	ENS (kWh)	0	1026.41	1613.2	1478.24	4117.85
MG 7	OC (\$)	98.77	5696.54	4367.47	24424.37	34587.15
	ENS (kWh)	0	904.76	709.87	3773.36	5387.99
MG 8	OC (\$)	2706.75	26605.48	26998.92	57531.63	113842.8
	ENS (kWh)	0	3781.76	3922.47	7961.5	15665.73
DSO	OC (\$)	6694.64	13777.68	12785.75	35397.31	68655.38
	ENS (kWh)	0	2415.68	2366.89	5398.71	10181.28
Sum	OC (\$)	11353.72	59274.56	63525.12	206677	340830.4
	ENS (kWh)	0	9419.76	10312.23	30824.47	50556.46

Table 10. Results obtained for the case 4.

Time Period		Pre-Disturbance (10:00-12:00)	During Disturbance (12:00-14:00)	Post-Disturbance (14:00-15:30)	Restoration (15:30-23:00)	Sum
MG 1	OC (\$)	-478.21	-437.73	-289.07	-715.62	-1920.63
	ENS (kWh)	0	0	0	0	0
MG 2	OC (\$)	81.72	1713.36	1220.88	5112.04	8128
	ENS (kWh)	0	304.14	246.65	924.45	1475.24
MG 3	OC (\$)	-544.71	-549.15	-377.11	-695.94	-2166.91
	ENS (kWh)	0	0	0	0	0
MG 4	OC (\$)	2310.44	2112.17	3346.93	57422.46	65192
	ENS (kWh)	0	67.5	298.38	7725.53	8091.41
MG 5	OC (\$)	188.25	4379.89	4382.73	17548.43	26499.3
	ENS (kWh)	0	919.51	915.52	3507.6	5342.63
MG 6	OC (\$)	296.07	5976.32	10150.77	12566.66	28989.82
	ENS (kWh)	0	1026.41	1751.57	1777.37	4555.35
MG 7	OC (\$)	98.77	5696.54	8971.63	22476.48	37243.42

	ENS (kWh)	0	904.76	1387.96	3482.62	5775.34
MG 8	OC (\$)	2706.75	26605.48	20315.66	48864.01	98491.9
	ENS (kWh)	0	3781.76	2940.67	6606.33	13328.76
DSO	OC (\$)	6694.64	13777.68	14078.11	33324.66	67875.09
	ENS (kWh)	0	2415.68	2624.27	4978.85	10018.8
Sum	OC (\$)	11353.72	59274.56	61800.53	195903.18	328332
	ENS (kWh)	0	9419.76	10165.02	29002.75	48587.53

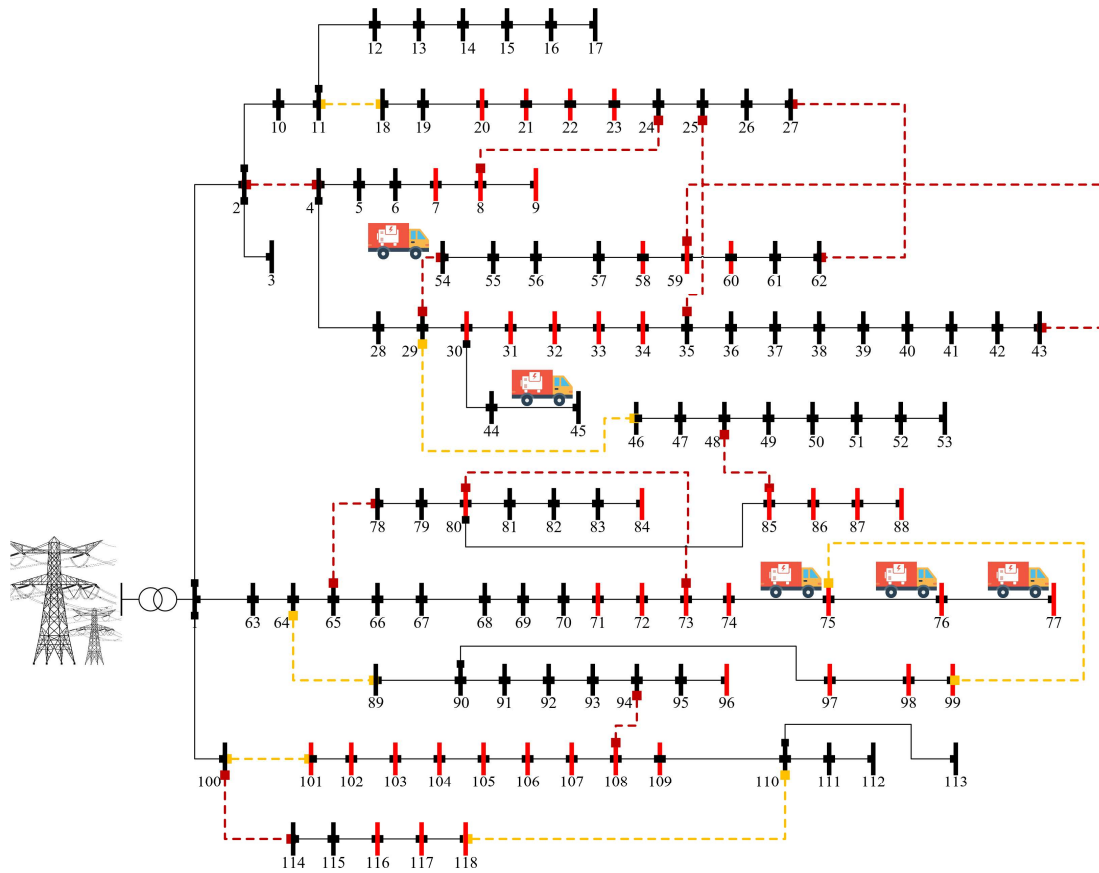


Fig. 8. Location of MEGs in the case 3.

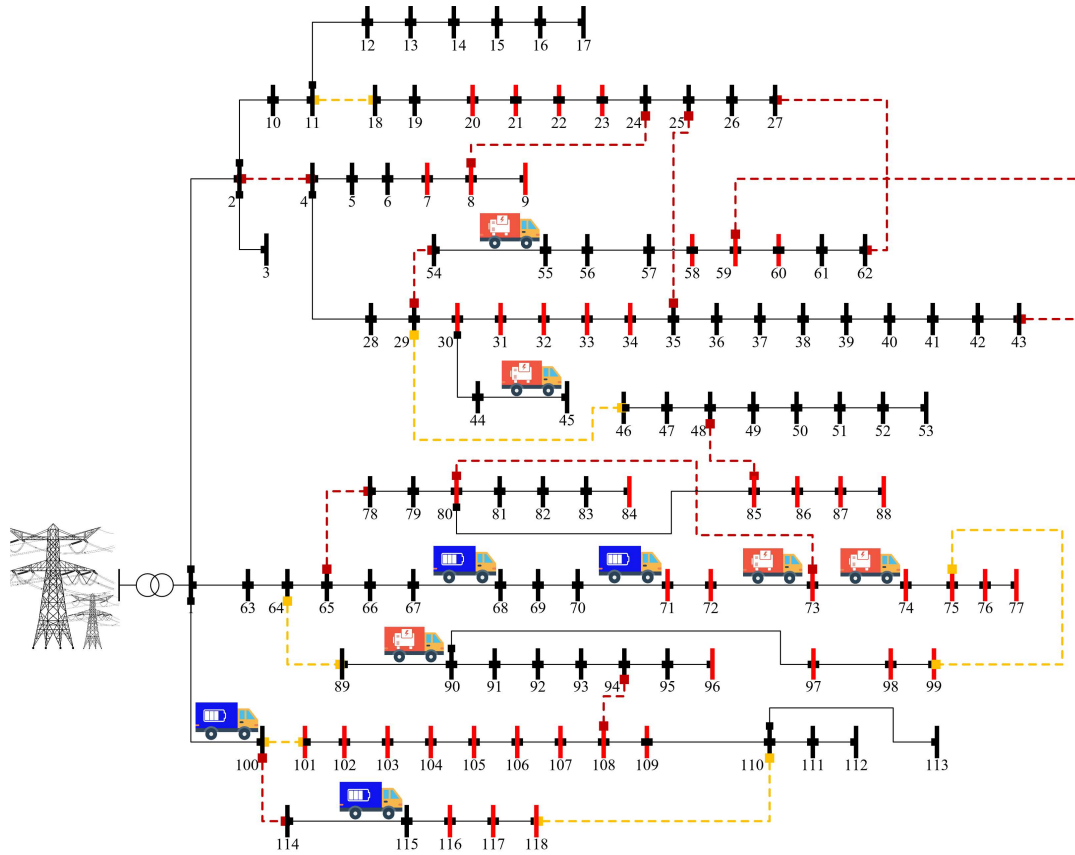


Fig. 9. Location of MEGs and MESSs in the case 4.

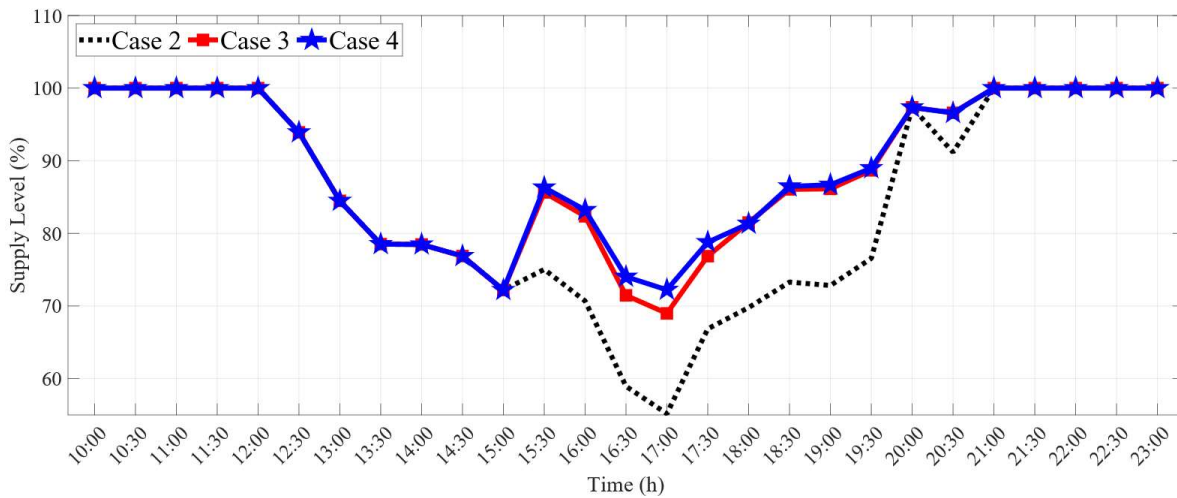


Fig. 10. Load supply curve in cases 2, 3 and 4.

4.4. Results of Cases 5 & 6

The results of case 5 are presented in Table 11. The proactive actions are performed before the occurrence of the disturbance to increase the resilience of the system in this case. In fact, these actions include DFR and dispatching mobile units from the depot to the stations. Figure 11 depicts the topology obtained for the network after performing proactive actions, where DSO

has changed the network topology according to the fault scenarios. Figure 12 depicts the route of mobile units and crew teams in the pre-disturbance phase. According to the figure, the crew teams have travelled from the depot to the location of the manual switches, and went to the stations after changing the status of the manual switches. This figure Further indicates that the mobile units are sent from the depot to the stations.

Table 12 indicates that performing proactive actions have reduced in ENS in the post-disturbance phase. Further, numerical results illustrate that the total operating cost and ENS are reduced by 6.74% and 8.44% compared to case 4 (without proactive actions), respectively. It is worth mentioning that these values are the sum of operating costs / ENS of MGs and DSOs. Figure 13 depicts the load supply curve in cases 4 and 5. In fact, the analysis of this figure indicates that at 14:30 and 15:00 the load supply level in case 5 is considerably higher than case 4, due to the faster connection of mobile units to the network in this case. Moreover, because of the stations are closer to the network buses than the depot, the mobile units in case 5 have connected to the network earlier than case 4 and thus injected more power into the network. Finally, Figure 14 depicts the power injected into the network by mobile units in cases 4 and 5, and this figure. indicates that the mobile units in case 5 started producing earlier than case 4.

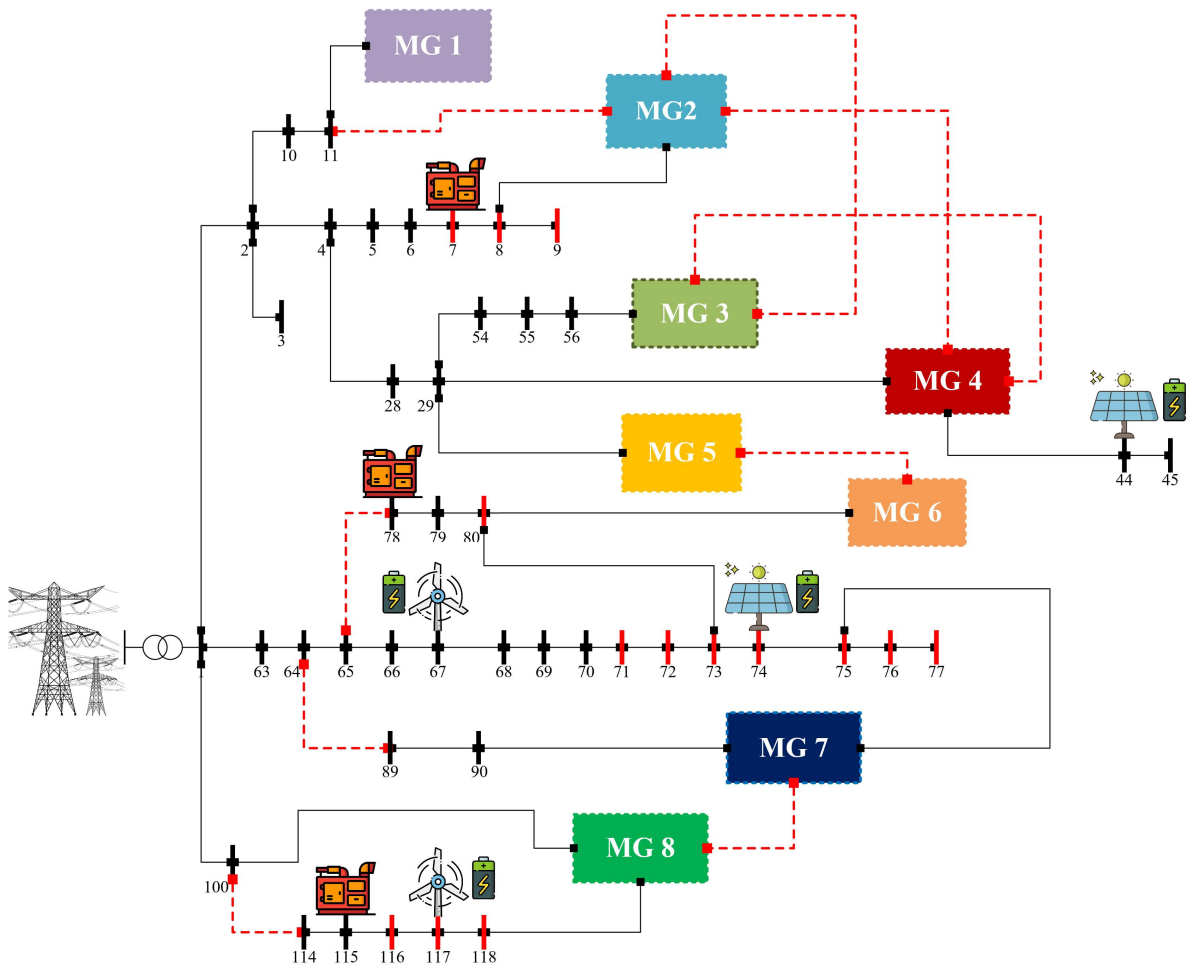


Fig. 11. Topology obtained for the network by considering proactive actions.

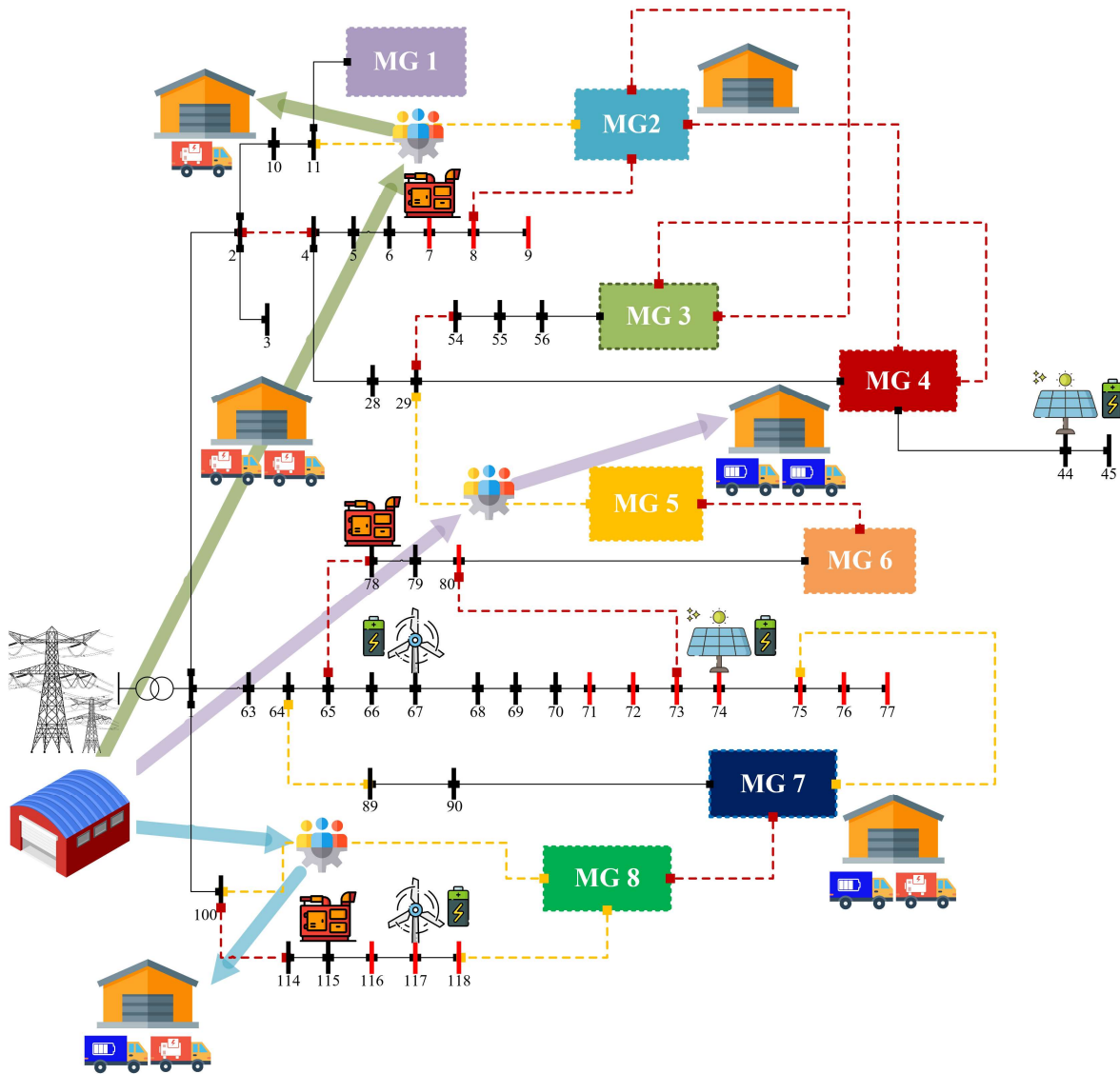


Fig. 12. The rout of mobile units and crew teams in the pre-disturbance phase in case 5

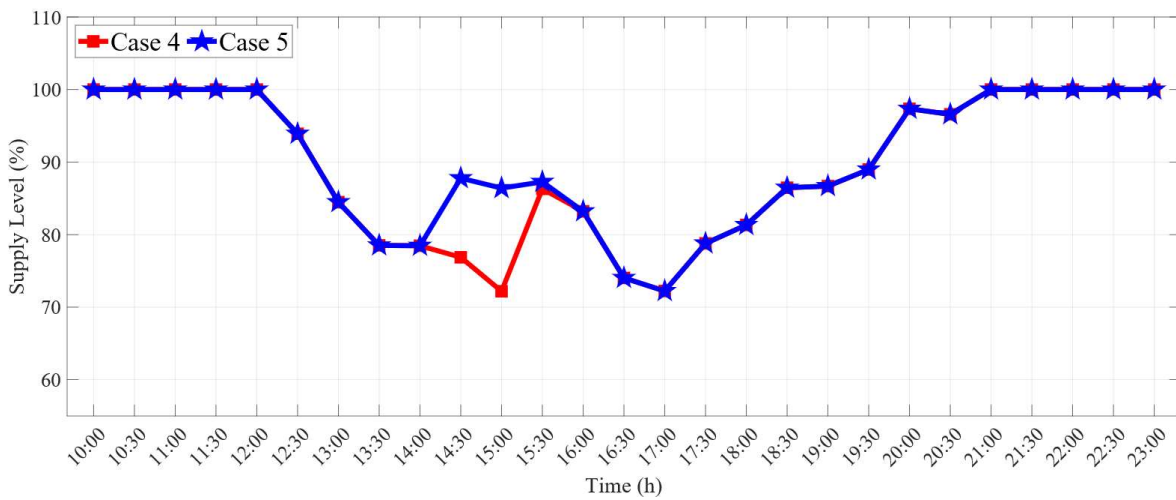


Fig. 13. Load supply curve in cases 4 and 5.

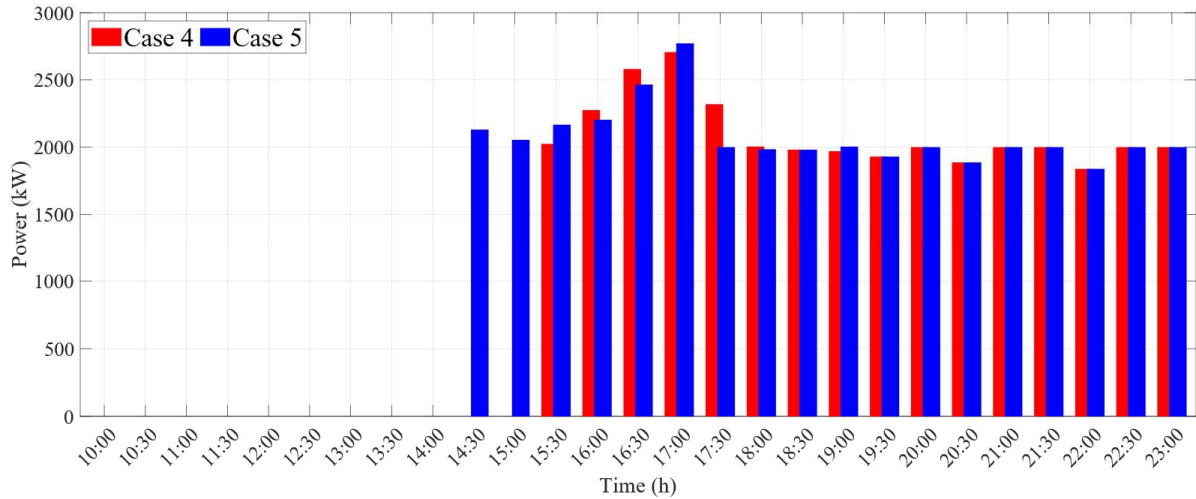


Fig. 14. Power injected into the network by mobile units in cases 4 and 5.

Table 11. Results obtained for the case 5.

Time Period		Pre-Disturbance (10:00-12:00)	During Disturbance (12:00-14:00)	Post-Disturbance (14:00-15:30)	Restoration (15:30-23:00)	Sum
MG 1	OC (\$)	-478.21	-443.43	-289.07	-715.62	-1926.33
	ENS (kWh)	0	0	0	0	0
MG 2	OC (\$)	81.72	478.93	1229.53	7682.63	9472.81
	ENS (kWh)	0	117.7	246.65	1301.78	1666.13
MG 3	OC (\$)	-544.71	-557.78	-375.31	-695.64	-2173.44
	ENS (kWh)	0	0	0	0	0
MG 4	OC (\$)	2310.44	2101.82	2204.43	52238.65	58855.34
	ENS (kWh)	0	67.5	127.2	7164.39	7359.09
MG 5	OC (\$)	188.25	4815.84	3675.98	17236.95	25917.02
	ENS (kWh)	0	1013.47	759.82	3444.31	5217.6
MG 6	OC (\$)	296.07	8575.57	6124.13	12250.28	27246.05
	ENS (kWh)	0	1464.49	906.96	1693.73	4065.18
MG 7	OC (\$)	98.77	5463.16	3224.95	23460.95	32247.83
	ENS (kWh)	0	895.31	507.6	3592.52	4995.43
MG 8	OC (\$)	2706.75	26424.56	18909.54	49427.81	97468.66
	ENS (kWh)	0	3768.12	2624.77	6582.26	12975.15
DSO	OC (\$)	6694.64	10249.19	6187.47	35959.55	59090.85
	ENS (kWh)	0	1710.66	990	5506.85	8207.51
Sum	OC (\$)	11353.72	57107.86	40891.65	196845.56	306198.8
	ENS (kWh)	0	9037.25	6163	29285.84	44486.09

Table 12 presents the results of case 6. In this case, the load type data are also shared by MGs in addition to power exchange data. The results indicate that the amount of ENS has increased

in the main grid and MGs 2,3 and 5, while the ENS has decreased in MGs 4, 6, 7 and 8. However, MGs 1 and 5 do not contain critical loads. Therefore, the results demonstrate that sharing load type data with DSO could increase the supply level of critical loads., Further, the supply of more critical loads in case 6 has led to a significant reduction in the operating costs of MGs 4, 6, 7 and 8 compared to case 5. Figure 15 depicts the ENS of regular and critical loads in different MGs, and the figure illustrate that the supply level of critical load in case 6 has increased significantly.

Figure 16 compares the resilience index in different cases, and this figure indicates that considering DFR in case 2 has increased the resilience index by r 3.16% compared to case 1. Moreover, the allocation of mobile units in case 4 has increased the resilience index by 3.9% compared to case 2 (in the absence of mobile units). Eventually, the sharing load type data by MGs in case 6 has resulted in a 3.47% growth in resilience index compared to case 5 (non-sharing of load type data). In addition, Fig. 17 depicts the order of repairing damaged lines in case 6 and the priority of repairing damaged lines is determined according to their impact on ENS. In other words, repair crews are allocated to reduce ENS.

Table 12. Results obtained for the case 6.

Time Period		Pre-Disturbance (10:00-12:00)	During Disturbance (12:00-14:00)	Post-Disturbance (14:00-15:30)	Restoration (15:30-23:00)	Sum
MG 1	OC (\$)	-478.21	-440.84	-292.18	-715.1	-1926.33
	ENS (kWh)	0	0	0	0	0
MG 2	OC (\$)	81.72	478.93	1229.53	7402.68	9192.86
	ENS (kWh)	0	117.7	246.65	1398.65	1763
MG 3	OC (\$)	-544.71	-557.78	-369.13	-396.34	-1867.96
	ENS (kWh)	0	0	0	63.58	63.58
MG 4	OC (\$)	2310.44	1646.71	1352.21	34892.47	40201.83
	ENS (kWh)	0	0	0	6146.62	6146.62
MG 5	OC (\$)	188.25	2517.71	3668.62	20486	26860.58
	ENS (kWh)	0	527.58	759.82	4120.68	5408.08
MG 6	OC (\$)	296.07	4361.43	5599	6514.41	16770.91
	ENS (kWh)	0	702.63	803.44	776.18	2282.25
MG 7	OC (\$)	98.77	5179.51	2456.75	9801.65	17536.68
	ENS (kWh)	0	965.46	521.1	1850.3	3336.86
MG 8	OC (\$)	2706.75	22109.91	14699.3	46180.95	85696.91

	ENS (kWh)	0	2986.65	1946.2	6010.87	10943.72
DSO	OC (\$)	6694.64	20384.51	10661.58	53107.12	90847.85
	ENS (kWh)	0	3737.23	1885.78	8918.98	14541.99
Sum	OC (\$)	11353.72	55680.09	39005.68	177273.84	283313.3
	ENS (kWh)	0	9037.25	6163	29285.84	44486.09

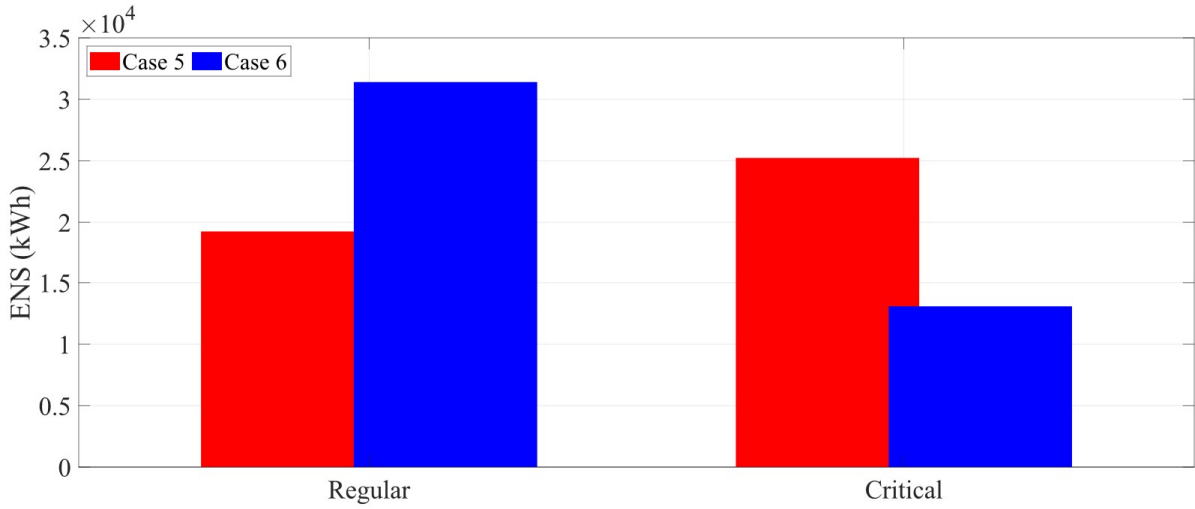


Fig. 15. ENS of regular and critical loads in cases 5 and 6.

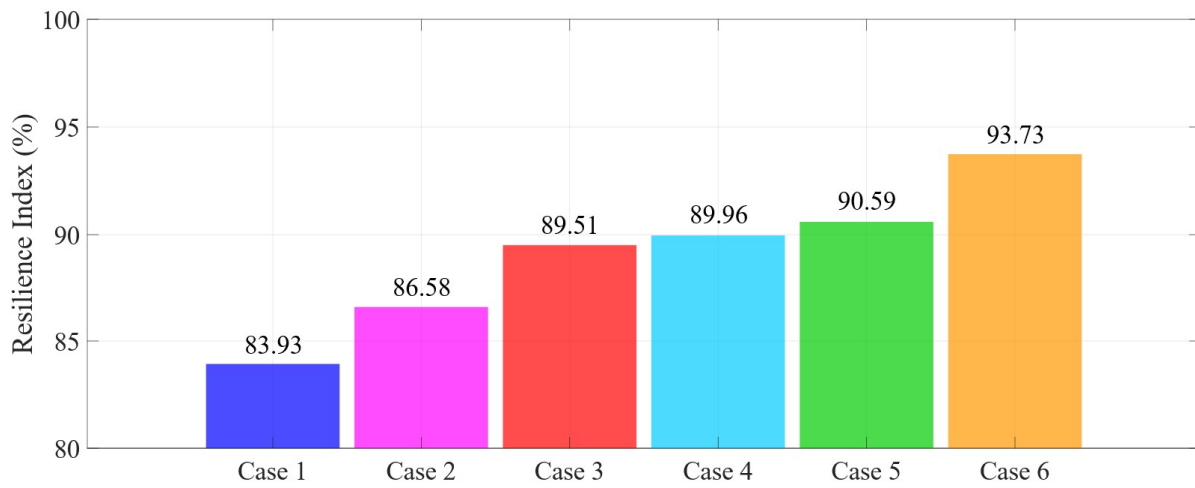


Fig. 16. Resilience index of the network in different cases.

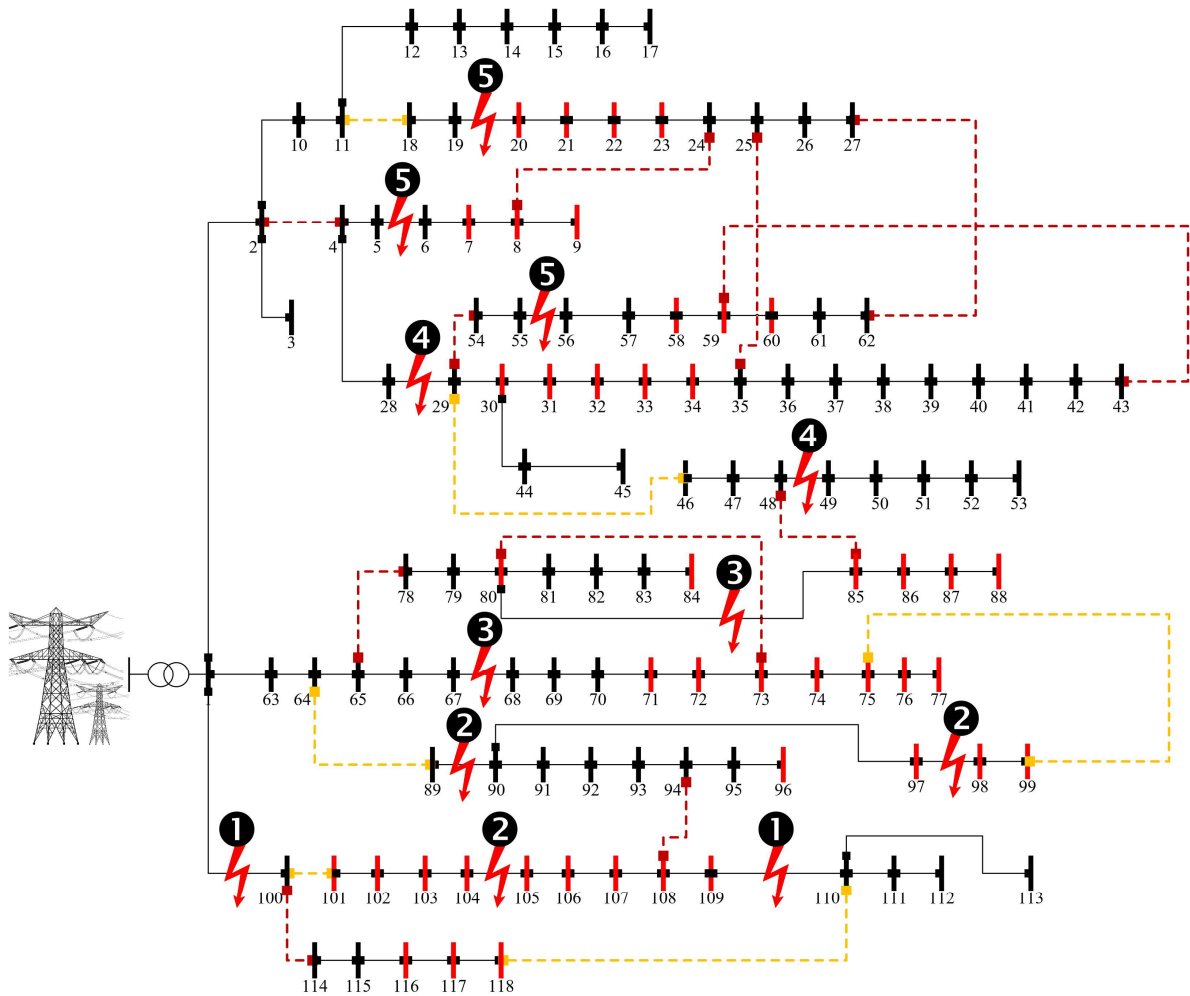


Fig. 17. Scheduling obtained for repair crews in restoration phase.

5. Discussion

In terms of mathematical point of view, the proposed model presents a hierarchical model which the solution space could decompose into several layers. This leads to a more accurate management of the operation problem and fragmentation of the solution space. Further, evaluating the proposed model from the resilience point of view shows that proactive actions, dynamic topology, dispatching of mobile units and increasing the level of data sharing among DC-MGs could improve the outage management of the system against extreme weather conditions. Moreover, the results show that one of the important points to prevent the spread of faults in the network is the timely prediction of upcoming events. In terms of the operational point of view, the proposed model indicates that timely prediction leads to the rapid scheduling

of proactive actions and increases the network readiness to deal with upcoming events. In addition, the results show that manual / automatic switches play a key role in rerouting power flow and preventing the spread of faults in the network. Finally, in terms of the security point of view, the study defines that the rate of information sharing among DC-MGs should change according to the operating conditions. In addition, the results clearly show that increasing the rate of information sharing during emergency conditions leads to the rescue of many critical loads.

On the other hand, one of the limitations in the proposed model is related to the modelling of the windstorm. It should be noted that the uncertain movement of the windstorm is not considered in the proposed model, and the wind speed throughout each region is considered constant. Therefore, dynamic modeling of the windstorm can be considered in future work to achieve more realistic results. In addition, the proposed model does not evaluate the effects of fault on system frequency, which also could be addressed in future work.

6. Conclusion

This paper presents a hierarchical framework for outage management of DC-MGs. Proactive actions, mobile unit allocation and DFR were considered to improve the system resilience in the proposed model. It should be noted that, system outage management was performed according to the data shared by MGs. Ultimately, the proposed model was implemented on a 118-bus distribution system and the results could be summarized as follows:

- The problem of outage management was solved by considering the dynamic topology, and the results showed that DSO rerouted the power flow by implementing DFR, thus reducing the ENS by 21.6%. Further, it also mirrored that DFR allows more utilization of DERs capacity.

- Routing and allocation of mobile units were considered in the model, and the results indicated that the participation of these units in load supply has led to a reduction of 30% and 26.3% in ENS and operating cost, respectively.
- The effect of proactive actions on system resilience was investigated, and the results demonstrated that performing proactive actions has led to a reduction in the installation time of mobile units and subsequently increased the resilience index of the system.
- The effects of MG data sharing on system resilience were examined, and the results confirmed that load type data sharing has led to a 48.16% increase in critical load supply.

In addition, the results testify that the proposed hierarchical model is an effective approach to enhance the resilience of DC-MGs. The future research suggestions could be presented as follows:

- 1- Enhance the resilience of interconnected MGs considering vehicle-to-grid services of EVs
- 2- Enhance the resilience of renewable-based MGs considering the translational movement of the windstorm
- 3- Introduce a hierarchical model to control the voltage and frequency of MGs during extreme weather conditions

Acknowledgments

This work was supported from DTE Network+ funded by EPSRC grant reference EP/S032053/1.

List of References

- [1] Jufri FH, Widiputra V, Jung J. State-of-the-art review on power grid resilience to extreme weather events: Definitions, frameworks, quantitative assessment methodologies, and enhancement strategies. *Appl Energy* 2019;239:1049–65. <https://doi.org/10.1016/j.apenergy.2019.02.017>.

- [2] Mishra DK, Ghadi MJ, Azizivahed A, Li L, Zhang J. A review on resilience studies in active distribution systems. *Renew Sustain Energy Rev* 2021;135:110201. <https://doi.org/https://doi.org/10.1016/j.rser.2020.110201>.
- [3] Huang G, Wang J, Chen C, Qi J, Guo C. Integration of Preventive and Emergency Responses for Power Grid Resilience Enhancement. *IEEE Trans Power Syst* 2017;32:4451–63. <https://doi.org/10.1109/TPWRS.2017.2685640>.
- [4] Hossain E, Roy S, Mohammad N, Nawar N, Dipta DR. Metrics and enhancement strategies for grid resilience and reliability during natural disasters. *Appl Energy* 2021;290:116709. <https://doi.org/https://doi.org/10.1016/j.apenergy.2021.116709>.
- [5] Wang Y, Rousis AO, Strbac G. A resilience enhancement strategy for networked microgrids incorporating electricity and transport and utilizing a stochastic hierarchical control approach. *Sustain Energy, Grids Networks* 2021;26:100464. <https://doi.org/https://doi.org/10.1016/j.segan.2021.100464>.
- [6] Wang Y, Rousis AO, Strbac G. Resilience-driven optimal sizing and pre-positioning of mobile energy storage systems in decentralized networked microgrids. *Appl Energy* 2022;305:117921. <https://doi.org/https://doi.org/10.1016/j.apenergy.2021.117921>.
- [7] Ali AY, Hussain A, Baek J-W, Kim H-M. Optimal Operation of Networked Microgrids for Enhancing Resilience Using Mobile Electric Vehicles. *Energies* 2021;14. <https://doi.org/10.3390/en14010142>.
- [8] Omogoye OS, Folly KA, Awodele KO. Review of Proactive Operational Measures for the Distribution Power System Resilience Enhancement Against Hurricane Events. 2021 South. African Univ. Power Eng. Conf. Mechatronics/Pattern Recognit. Assoc. South Africa, 2021, p. 1–6. <https://doi.org/10.1109/SAUPEC/RobMech/PRASA52254.2021.9377252>.
- [9] Taheri B, Safdarian A, Moeini-Aghaie M, Lehtonen M. Enhancing Resilience Level of

- Power Distribution Systems Using Proactive Operational Actions. *IEEE Access* 2019;7:137378–89. <https://doi.org/10.1109/ACCESS.2019.2941593>.
- [10] Lei S, Chen C, Zhou H, Hou Y. Routing and Scheduling of Mobile Power Sources for Distribution System Resilience Enhancement. *IEEE Trans Smart Grid* 2019;10:5650–62. <https://doi.org/10.1109/TSG.2018.2889347>.
- [11] Mehrjerdi H, Mahdavi S, Hemmati R. Resilience maximization through mobile battery storage and diesel DG in integrated electrical and heating networks. *Energy* 2021;121195. <https://doi.org/https://doi.org/10.1016/j.energy.2021.121195>.
- [12] Dehghani NL, Jeddi AB, Shafieezadeh A. Intelligent hurricane resilience enhancement of power distribution systems via deep reinforcement learning. *Appl Energy* 2021;285:116355. <https://doi.org/https://doi.org/10.1016/j.apenergy.2020.116355>.
- [13] Venkateswaran V B, Saini DK, Sharma M. Techno-economic hardening strategies to enhance distribution system resilience against earthquake. *Reliab Eng Syst Saf* 2021;213:107682. <https://doi.org/https://doi.org/10.1016/j.res.2021.107682>.
- [14] Li B, Chen Y, Wei W, Huang S, Xiong Y, Mei S, et al. Routing and Scheduling of Electric Buses for Resilient Restoration of Distribution System. *IEEE Trans Transp Electrif* 2021;7:2414–28. <https://doi.org/10.1109/TTE.2021.3061079>.
- [15] Omogoye OS, Folly KA, Awodele KO. Review of Sequential Steps to Realize Power System Resilience. 2020 Int. SAUPEC/RobMech/PRASA Conf., 2020, p. 1–6. <https://doi.org/10.1109/SAUPEC/RobMech/PRASA48453.2020.9040967>.
- [16] Cai S, Xie Y, Wu Q, Xiang Z. Robust MPC-based microgrid scheduling for resilience enhancement of distribution system. *Int J Electr Power Energy Syst* 2020;121:106068. <https://doi.org/https://doi.org/10.1016/j.ijepes.2020.106068>.
- [17] Shi Q, Li F, Olama M, Dong J, Xue Y, Starke M, et al. Network reconfiguration and distributed energy resource scheduling for improved distribution system resilience. *Int*

- J Electr Power Energy Syst 2021;124:106355.
<https://doi.org/https://doi.org/10.1016/j.ijepes.2020.106355>.
- [18] Erenoğlu AK, Erdinç O. Post-Event restoration strategy for coupled distribution-transportation system utilizing spatiotemporal flexibility of mobile emergency generator and mobile energy storage system. *Electr Power Syst Res* 2021;199:107432. <https://doi.org/10.1016/j.epsr.2021.107432>.
- [19] Dabbaghjamanesh M, Senemmar S, Zhang J. Resilient Distribution Networks Considering Mobile Marine Microgrids: A Synergistic Network Approach. *IEEE Trans Ind Informatics* 2021;17:5742–50. <https://doi.org/10.1109/tii.2020.2999326>.
- [20] Jiang X, Chen J, Wu Q, Zhang W, Zhang Y, Liu J. Two-step Optimal Allocation of Stationary and Mobile Energy Storage Systems in Resilient Distribution Networks. *J Mod Power Syst Clean Energy* 2021;9:788–99. <https://doi.org/10.35833/mpce.2020.000910>.
- [21] Hughes W, Zhang W, Bagtzoglou AC, Wanik D, Pensado O, Yuan H, et al. Damage modeling framework for resilience hardening strategy for overhead power distribution systems. *Reliab Eng Syst Saf* 2021;207:107367. <https://doi.org/10.1016/j.res.2020.107367>.
- [22] Zhang G, Zhang F, Wang X, Zhang X. Fast Resilience Assessment of Distribution Systems with a Non-Simulation-Based Method. *IEEE Trans Power Deliv* 2021;1. <https://doi.org/10.1109/tpwr.2021.3077239>.
- [23] Ghasemi M, Kazemi A, Bompard E, Aminifar F. A two-stage resilience improvement planning for power distribution systems against hurricanes. *Int J Electr Power Energy Syst* 2021;132:107214. <https://doi.org/https://doi.org/10.1016/j.ijepes.2021.107214>.
- [24] Sedgh SA, Doostizadeh M, Aminifar F, Shahidehpour M. Resilient-enhancing critical load restoration using mobile power sources with incomplete information. *Sustain*

- Energy, Grids Networks 2021;26:100418. <https://doi.org/10.1016/j.segan.2020.100418>.
- [25] Ding T, Qu M, Wang Z, Chen B, Chen C, Shahidehpour M. Power System Resilience Enhancement in Typhoons Using a Three-Stage Day-Ahead Unit Commitment. *IEEE Trans Smart Grid* 2021;12:2153–64. <https://doi.org/10.1109/tsg.2020.3048234>.
- [26] Gharehveran SS, Ghassemzadeh S, Rostami N. Two-stage resilience-constrained planning of coupled multi-energy microgrids in the presence of battery energy storages. *Sustain Cities Soc* 2022;83:103952. <https://doi.org/10.1016/j.scs.2022.103952>.
- [27] Jia L, Kandaperumal G, Pannala S, Srivastava A. Coordinating Energy Resources in an Islanded Microgrid for Economic and Resilient Operation. 2021 IEEE Ind Appl Soc Annu Meet 2021. <https://doi.org/10.1109/ias48185.2021.9677050>.
- [28] Jahromi SN, Hajipour E, Ehsan M. Optimal Resilience-Oriented Microgrid Formation Considering Failure Probability of Distribution Feeders. *Electr Power Syst Res* 2022;209:108012. <https://doi.org/10.1016/j.epsr.2022.108012>.
- [29] Gilani MA, Dashti R, Ghasemi M, Amirioun MH, Shafie-khah M. A Microgrid Formation-Based Restoration Model for Resilient Distribution Systems Using Distributed Energy Resources and Demand Response Programs. *SSRN Electron J* 2022. <https://doi.org/10.2139/ssrn.4046621>.
- [30] Jiang L, Li X, Long T, Zhou R, Jiang J, Bie Z, et al. Resilient service restoration for distribution systems with mobile resources using Floyd-based network simplification method. *IET Gener Transm & Distrib* 2021;16:414–29. <https://doi.org/10.1049/gtd2.12290>.
- [31] Wu H, Xie Y, Xu Y, Wu Q, Yu C, Sun J. Resilient scheduling of MESSs and RCs for distribution system restoration considering the forced cut-off of wind power. *Energy* 2022;244:123081. <https://doi.org/10.1016/j.energy.2021.123081>.
- [32] Xin N, Chen L, Ma L, Si Y. A Rolling Horizon Optimization Framework for Resilient

- Restoration of Active Distribution Systems. *Energies* 2022;15:3096.
<https://doi.org/10.3390/en15093096>.
- [33] Li Z, Tang W, Lian X, Chen X, Zhang W, Qian T. A resilience-oriented two-stage recovery method for power distribution system considering transportation network. *Int J Electr Power Energy Syst* 2022;135:107497.
<https://doi.org/10.1016/j.ijepes.2021.107497>.
- [34] Mansouri SA, Nematbakhsh E, Javadi MS, Jordehi AR, Shafie-khah M, Catalão JPS. Resilience Enhancement via Automatic Switching considering Direct Load Control Program and Energy Storage Systems. 2021 IEEE Int. Conf. Environ. Electr. Eng. 2021 IEEE Ind. Commer. Power Syst. Eur. (EEEIC / I&CPS Eur., 2021, p. 1–6.
<https://doi.org/10.1109/EEEIC/ICPSEurope51590.2021.9584609>.
- [35] Zhang D, Fu Z, Zhang L. An improved TS algorithm for loss-minimum reconfiguration in large-scale distribution systems. *Electr Power Syst Res* 2007;77:685–94.
<https://doi.org/10.1016/j.epsr.2006.06.005>.
- [36] Gutiérrez Galeano A, Bressan M, Jiménez Vargas F, Alonso C. Shading Ratio Impact on Photovoltaic Modules and Correlation with Shading Patterns. *Energies* 2018;11:852.
<https://doi.org/10.3390/en11040852>.
- [37] Mansouri SA, Ahmarinejad A, Nematbakhsh E, Javadi MS, Jordehi AR, Catalão JPS. Energy Management in Microgrids including Smart Homes: A Multi-objective Approach. *Sustain Cities Soc* 2021:102852.
<https://doi.org/https://doi.org/10.1016/j.scs.2021.102852>.
- [38] Yuan H, Li F, Wei Y, Zhu J. Novel Linearized Power Flow and Linearized OPF Models for Active Distribution Networks With Application in Distribution LMP. *IEEE Trans Smart Grid* 2018;9:438–48. <https://doi.org/10.1109/TSG.2016.2594814>.
- [39] Ma S, Su L, Wang Z, Qiu F, Guo G. Resilience Enhancement of Distribution Grids

- Against Extreme Weather Events. *IEEE Trans Power Syst* 2018;33:4842–53. <https://doi.org/10.1109/TPWRS.2018.2822295>.
- [40] Jooshaki M, Abbaspour A, Fotuhi-Firuzabad M, Muñoz-Delgado G, Contreras J, Lehtonen M, et al. Linear Formulations for Topology-Variable-Based Distribution System Reliability Assessment Considering Switching Interruptions. *IEEE Trans Smart Grid* 2020;11:4032–43. <https://doi.org/10.1109/TSG.2020.2991661>.
- [41] Amir Mansouri S, Javadi MS, Ahmarinejad A, Nematbakhsh E, Zare A, Catalão JPS. A coordinated energy management framework for industrial, residential and commercial energy hubs considering demand response programs. *Sustain Energy Technol Assessments* 2021;47:101376. <https://doi.org/10.1016/j.seta.2021.101376>.
- [42] Taheri B, Safdarian A, Moeini-Aghaie M, Lehtonen M. Distribution System Resilience Enhancement via Mobile Emergency Generators. *IEEE Trans Power Deliv* 2020;1. <https://doi.org/10.1109/TPWRD.2020.3007762>.
- [43] Lin Y, Chen B, Wang J, Bie Z. A Combined Repair Crew Dispatch Problem for Resilient Electric and Natural Gas System Considering Reconfiguration and DG Islanding. *IEEE Trans Power Syst* 2019;34:2755–67. <https://doi.org/10.1109/TPWRS.2019.2895198>.
- [44] Lei S, Chen C, Li Y, Hou Y. Resilient Disaster Recovery Logistics of Distribution Systems: Co-Optimize Service Restoration With Repair Crew and Mobile Power Source Dispatch. *IEEE Trans Smart Grid* 2019;10:6187–202. <https://doi.org/10.1109/TSG.2019.2899353>.
- [45] Jose J, Kowli A. Path-Based Distribution Feeder Reconfiguration for Optimization of Losses and Reliability. *IEEE Syst J* 2020;14:1417–26. <https://doi.org/10.1109/JSYST.2019.2917536>.
- [46] Mansouri SA, Ahmarinejad A, Javadi MS, Catalão JPS. Two-stage stochastic framework for energy hubs planning considering demand response programs. *Energy*

2020;206:118124. <https://doi.org/10.1016/j.energy.2020.118124>.